

2018-04-11

JIP1-Mediated JNK Activation Negatively Regulates Synaptic Plasticity and Spatial Memory

Caroline Morel
University of Massachusetts Medical School

Et al.

Let us know how access to this document benefits you.

Follow this and additional works at: https://escholarship.umassmed.edu/faculty_pubs



Part of the Amino Acids, Peptides, and Proteins Commons, Cell Biology Commons, Cellular and Molecular Physiology Commons, Developmental Biology Commons, Enzymes and Coenzymes Commons, Molecular and Cellular Neuroscience Commons, and the Molecular Biology Commons

Repository Citation

Morel C, Sherrin T, Kennedy NJ, Forest KH, Barutcu S, Robles M, Carpenter-Hyland E, Alfulaij N, Standen CL, Nichols RA, Benveniste M, Davis RJ, Todorovic C. (2018). JIP1-Mediated JNK Activation Negatively Regulates Synaptic Plasticity and Spatial Memory. University of Massachusetts Medical School Faculty Publications. <https://doi.org/10.1523/JNEUROSCI.1913-17.2018>. Retrieved from https://escholarship.umassmed.edu/faculty_pubs/1492

This material is brought to you by eScholarship@UMMS. It has been accepted for inclusion in University of Massachusetts Medical School Faculty Publications by an authorized administrator of eScholarship@UMMS. For more information, please contact Lisa.Palmer@umassmed.edu.

Research Articles: Cellular/Molecular

JIP1-Mediated JNK Activation Negatively Regulates Synaptic Plasticity and Spatial Memory

Caroline Morel^{1,2}, Tessi Sherrin³, Norman J. Kennedy^{1,2}, Kelly H Forest³, Seda Avcioglu Barutcu^{1,2}, Michael Robles³, Ezekiel Carpenter-Hyland⁴, Naghum Alfulaj³, Claire L. Standen^{1,2}, Robert A. Nichols³, Morris Benveniste⁴, Roger J. Davis^{1,2} and Cedomir Todorovic³

¹Howard Hughes Medical Institute

²Program in Molecular Medicine, University of Massachusetts Medical School, 373 Plantation Street, Worcester, MA 01605, USA.

³Department of Cell & Molecular Biology, John A Burns School of Medicine, University of Hawaii, 651 Ilalo St, Honolulu, HI, 96813, USA.

⁴Neuroscience Institute, Morehouse School of Medicine, 720 Westview Drive, SW, Atlanta, GA, 30310, USA.

DOI: 10.1523/JNEUROSCI.1913-17.2018

Received: 7 July 2017

Revised: 6 February 2018

Accepted: 3 March 2018

Published: 14 March 2018

Author contributions: C.T., C.M., and T.S. wrote the first draft of the paper; N.K. and R.J.D. edited the paper. C.T., C.M., T.S., N.K., M.B., and R.J.D. designed research; C.T., C.M., T.S., N.K., M.R., E.P.C.-H., N.A., C.S., K.H.F., and S.A.B. performed research; C.T., C.M., T.S., N.K., R.A.N., M.B., and R.J.D. analyzed data; C.T., N.K., R.A.N., M.B., and R.J.D. wrote the paper.

Conflict of Interest: The authors declare no competing financial interests.

We thank Tamera Barrett for technical assistance and Kathy Gemme for administrative assistance. These studies were supported by NIH grants U54MD008149 and MH086733 (CT) and by NIH grants S11NS055883, U54NS083932, and SC1AG046907 (MB). The behavior and electrophysiology core at the University of Hawaii was supported by NIH grant G12MD007601. RJD is an investigator of the Howard Hughes Medical Institute.

Correspondence should be addressed to Cedomir Todorovic, Department of Cell & Molecular Biology, John A Burns School of Medicine, University of Hawaii, 631 Ilalo St, Honolulu, HI, 96813, USA. University of Hawaii, 96813, USA. E-mail: cedomir@hawaii.edu, or to Roger J Davis, Howard Hughes Medical Institute and Program in Molecular Medicine, University of Massachusetts Medical School, 373 Plantation Street, Worcester, MA 01605, USA. E-mail: roger.davis@umassmed.edu

Cite as: J. Neurosci ; 10.1523/JNEUROSCI.1913-17.2018

Alerts: Sign up at www.jneurosci.org/cgi/alerts to receive customized email alerts when the fully formatted version of this article is published.

Accepted manuscripts are peer-reviewed but have not been through the copyediting, formatting, or proofreading process.

Copyright © 2018 the authors

JIP1-Mediated JNK Activation Negatively Regulates Synaptic Plasticity and Spatial Memory

Running Title: JIP1-regulated JNK and memory

Caroline Morel^{1,2,*}, Tessi Sherrin^{3,*}, Norman J. Kennedy^{1,2}, Kelly H Forest³, Seda Avcioglu Barutcu^{1,2}, Michael Robles³, Ezekiel Carpenter-Hyland⁴, Naghum Alfulajj³, Claire L. Standen^{1,2}, Robert A. Nichols³, Morris Benveniste⁴, Roger J. Davis^{1,2,**}, and Cedimir Todorovic^{3,**}

¹ Howard Hughes Medical Institute, ² Program in Molecular Medicine, University of Massachusetts Medical School, 373 Plantation Street, Worcester, MA 01605, USA.

³ Department of Cell & Molecular Biology, John A Burns School of Medicine, University of Hawaii, 651 Ilalo St, Honolulu, HI, 96813, USA.

⁴ Neuroscience Institute, Morehouse School of Medicine, 720 Westview Drive, SW, Atlanta, GA, 30310, USA.

Number of Pages: 52

Number of Figures: 14

Number of Words: (Abstract: 125; Introduction: 593; Discussion: 1490)

* CM and TS contributed equally to this work

** RJD and CT contributed equally to this work

Submitting author: Cedimir Todorovic, Department of Cell & Molecular Biology, John A Burns School of Medicine, University of Hawaii, 631 Ilalo St, Honolulu, HI, 96813, USA. University of Hawaii, 96813, USA. E-mail: cedomir@hawaii.edu

Correspondence should be addressed to Cedimir Todorovic, Department of Cell & Molecular Biology, John A Burns School of Medicine, University of Hawaii, 631 Ilalo St, Honolulu, HI, 96813, USA. University of Hawaii, 96813, USA. E-mail: cedomir@hawaii.edu, or to Roger J Davis, Howard Hughes Medical Institute and Program in Molecular Medicine, University of Massachusetts Medical School, 373 Plantation Street, Worcester, MA 01605, USA. E-mail: roger.davis@umassmed.edu

Conflict of Interest: The authors declare no competing financial interests.

Acknowledgements. We thank Tamera Barrett for technical assistance and Kathy Gemme for administrative assistance. These studies were supported by NIH grants U54MD008149 and MH086733 (CT) and by NIH grants S11NS055883, U54NS083932, and SC1AG046907 (MB). The behavior and electrophysiology core at the University of Hawaii was supported by NIH grant G12MD007601. RJD is an investigator of the Howard Hughes Medical Institute.

1 Abstract

2 The c-Jun N-terminal kinase (JNK) signal transduction pathway is implicated in learning and
3 memory. Here, we examined the role of JNK activation mediated by the JIP1 scaffold protein.
4 We compared male wild-type mice with a mouse model harboring a point mutation in the *Jip1*
5 gene that selectively blocks JIP1-mediated JNK activation. These male mutant mice exhibited
6 increased NMDA receptor currents, increased NMDA receptor-mediated gene expression, and
7 a lower threshold for induction of hippocampal long-term potentiation. The JIP1 mutant mice
8 also displayed improved hippocampus-dependent spatial memory and enhanced associative
9 fear conditioning. These results were confirmed using a second JIP1 mutant mouse model that
10 suppresses JNK activity. Together, these observations establish that JIP1-mediated JNK
11 activation contributes to the regulation of hippocampus-dependent, NMDA receptor-mediated
12 synaptic plasticity and learning.

13

14 Significance Statement

15 The results of this study demonstrate that JNK activation induced by the JIP1 scaffold protein
16 negatively regulates the threshold for induction of long-term synaptic plasticity through the
17 NMDA-type glutamate receptor. This change in plasticity threshold influences learning. Indeed,
18 mice with defects in JIP1-mediated JNK activation display enhanced memory in hippocampus-
19 dependent tasks, such as contextual fear conditioning and Morris water maze, indicating that
20 JIP1-JNK constrains spatial memory. This study reports the identification of JIP1-mediated JNK
21 activation as a novel molecular pathway that negatively regulates NMDA receptor-dependent
22 synaptic plasticity and memory.

23

24 Introduction

25 Human genetic studies have demonstrated that mutations in genes underlying the cJun NH₂-
26 terminal kinase (JNK) signaling pathway are associated with neuropsychiatric, neurological and
27 neurodevelopmental disorders, including schizophrenia (*MAP2K7*) (Winchester et al., 2012),
28 epilepsy (*MAPK10*) (Shoichet et al., 2006), autism spectrum disorder (*MAPK8IP2* & *TAOK2*)
29 (Weiss et al., 2008; Giza et al., 2010; de Anda et al., 2012), and learning disability (*MAPK10*)
30 (Baptista et al., 2008; Kunde et al., 2013). These observations suggest that the JNK pathway
31 has an important normal function in the central nervous system (CNS). Indeed, recent studies
32 using *C. elegans* (Inoue et al., 2013) and murine (Sherrin et al., 2011) experimental models
33 showed that JNK-deficiency results in enhanced memory. This is exemplified by the
34 observations that JNK1-deficient mice exhibit enhanced associative learning, including
35 contextual fear conditioning (Sherrin et al., 2010) and altered synaptic plasticity (Li et al., 2007).
36 Complementary studies using pharmacological inhibition of JNK demonstrate increased long-
37 term depression (LTD) and loss of depotentiation (Yang et al., 2011). Moreover, JNK activation
38 has been implicated in stress-mediated inhibition of long-term potentiation (LTP) (Curran et al.,
39 2003; Wang et al., 2004). Mechanisms that contribute to JNK-regulated synaptic plasticity
40 include NMDA receptor-stimulated JNK activation (Mukherjee et al., 1999), AMPA receptor
41 internalization (Zhu et al., 2005), and synaptic recruitment of PSD95 (Kim et al., 2007).
42 Collectively, these data indicate that JNK plays a key role in the regulation of synaptic plasticity.

43 Although progress towards understanding the role of JNK in neuronal signaling has been
44 achieved, little is known about the mechanisms that regulate JNK during behavioral responses.
45 Previous studies have implicated roles for scaffold proteins in the control of MAP kinase
46 signaling cascades, including the JNK signaling pathway (Morrison and Davis, 2003). Indeed,
47 the JNK-interacting protein 1 (JIP1) scaffold protein can assemble a functional JNK signaling

48 pathway (Whitmarsh et al., 1998; Whitmarsh et al., 2001). JIP1 is required for JNK activation
49 caused by specific stimuli, including metabolic and excitotoxic stress (Whitmarsh et al., 2001;
50 Morel et al., 2010). However, JIP1 is not required for JNK activation caused by other stimuli,
51 including inflammatory cytokines (Whitmarsh et al., 2001).

52 JIP1 is highly expressed in the brain (Dickens et al., 1997; Whitmarsh et al., 1998) and
53 localizes to synapses (Pellet et al., 2000). Interestingly, mice with JIP1-deficiency exhibit
54 increased NMDA receptor signaling (Kennedy et al., 2007), implicating JIP1-mediated JNK
55 activation in the regulation of NMDA receptor activity. The purpose of this study was to examine
56 the impact of JIP1-regulated JNK activation on neuronal function and behavior. JIP1 may
57 contribute to multiple biological processes, including microtubule motor protein function and JNK
58 signaling (Morrison and Davis, 2003). The interpretation of studies using JIP1 knockout mice
59 (Whitmarsh et al., 2001) is therefore complicated by the presence of defects in JIP1-mediated
60 JNK activation and defects in other JIP1-mediated biochemical activities. Consequently, we
61 examined the effect of a point mutation in JIP1 (Thr¹⁰³Ala) that selectively prevents JIP1-
62 mediated JNK activation (Morel et al., 2010). This block in JNK activation is accounted for by a
63 required role of JIP1 phosphorylation on Thr¹⁰³ for dynamic association with upstream MAP3K
64 components of the signaling cascade (Nihalani et al., 2003; Morel et al., 2010). Our results
65 demonstrated that JIP1-mediated JNK activation regulates hippocampus-dependent, NMDA
66 receptor-linked synaptic plasticity and memory. This conclusion was confirmed using a second
67 mouse model with point mutations that disrupt the JNK binding site on JIP1, which also prevents
68 JIP1-mediated JNK activation and alters hippocampus-dependent learning. Collectively, the
69 data demonstrate that the JIP1-JNK signaling axis negatively regulates synaptic plasticity and
70 spatial memory, possibly functioning to constrain and/or shape learning and memory under
71 specific contexts.

72

73 **Materials and Methods**

74

75 **Mice**

76 C57BL/6J mice (stock number 000664) were obtained from the Jackson Laboratory and were
77 established as a colony in our facility. The *Jip1 Thr¹⁰³Ala* (JIP1^{TA}) mice have been described
78 previously (Morel et al., 2010). Mice with a defect in the JNK binding domain of JIP1
79 (replacement of Leu¹⁶⁰-Asn¹⁶¹-Leu¹⁶² with Gly¹⁶⁰-Arg¹⁶¹-Gly¹⁶²) were established by homologous
80 recombination in embryonic stem (ES) cells using standard methods. The mutated allele is
81 designated as *Jip1^{ΔJBD}*. Briefly, a targeting vector was constructed that was designed to
82 introduce point mutations in exon 3 of the *Jip1* gene to create the ΔJBD mutation. TC1
83 embryonic stem cells (strain129svev) (RRID:CVCL_M350) were electroporated with this vector
84 and selected with 200 μg/ml G418 (Thermo Fisher Scientific, Cat# 10131035) and 2 μM
85 ganciclovir (Millipore, Cat# 345700). ES cell clones without (genotype *+/NeoR-Jip1^{WT}*) and with
86 (genotype *+/NeoR-Jip1^{ΔJBD}*) the ΔJBD mutation in exon 3 were identified. These ES cells were
87 injected into C57BL/6J blastocysts to create chimeric mice that were bred to obtain germ-line
88 transmission of the targeted *Jip1* allele. The floxed *Neo^R* cassette was excised using Cre
89 recombinase. The full characterization of these mice has been described elsewhere (Kant et
90 al., 2017). All mice used in this study were backcrossed (ten generations) to the C57BL/6J
91 strain (Jackson Laboratories). All studies were performed using male mice. The mice were
92 housed in a facility accredited by the American Association for Laboratory Animal Care
93 (AALAC). The Institutional Animal Care and Use Committee (IACUC) of the University of
94 Massachusetts, University of Hawaii, and Morehouse School of Medicine approved all studies
95 using animals.

96

97 **Primary hippocampal neurons**

98 Embryonic day 16.5 mouse embryos were used for isolation of primary hippocampal neurons

99 (Whitmarsh et al., 2001). Briefly, hippocampi were placed in ice-cold Hank's buffered saline
100 solution containing 20 mM HEPES (pH 7.3; HBSS, Thermo Fisher Scientific, Cat# 15630080)
101 and digested with 1% Trypsin (Thermo Fisher Scientific, Cat# 17075029) in the presence of 1
102 mg/mL DNase I (Sigma, Cat# 11284932001). The trypsin solution was removed, and the
103 minced tissue was triturated in 1.0 mL of HBSS-20mM HEPES containing DNase I (1 mg/mL)
104 (Sigma, Cat# 11284932001) and soybean trypsin inhibitor (0.5 mg/mL) (Thermo Fisher
105 Scientific, Cat# 17075029) to obtain a single-cell suspension. Dissociated neurons were
106 centrifuged (180g, 10 min, 4°C) through a cushion of 4% bovine serum albumin (BSA) (Thermo
107 Fisher Scientific, Cat# B14) in HBSS. Hippocampal neurons were seeded in poly-D-
108 lysine/laminin-coated chamber slides (BD Biosciences, Cat# 354687) in Neurobasal medium
109 (Thermo Fisher Scientific, Cat# 21103049) containing B27 supplement (Thermo Fisher
110 Scientific, Cat# 17504044), 1% glutamine (Thermo Fisher Scientific, Cat# 21051024), and 1%
111 penicillin/streptomycin (Thermo Fisher Scientific, Cat# 15140122).

112 Gene expression studies were performed using hippocampal neurons cultured for 14
113 days *in vitro* (14DIV). The neurons were treated without or with 100 μ M NMDA/10 μ M Glycine
114 (Sigma, Cat# M3262, Cat# G5417) in complete Neurobasal media (Thermo Fisher Scientific,
115 Cat# 21103049). The expression of mRNA was measured by quantitative RT-PCR assays.

116 Immunofluorescence analysis was performed using hippocampal neurons cultured for 16
117 days *in vitro* (16DIV). Two different procedures were used to prepare neurons for
118 immunofluorescence analysis. First, permeabilized fixed neurons were prepared by incubation
119 with 4% (w/v) paraformaldehyde (Thermo Fisher Scientific, Cat# 28906) at room temperature
120 (20 min) followed by incubation with 0.1% Triton X-100 in PBS (5 min) (Thermo Fisher
121 Scientific, Cat# 85112), and then blocking buffer (1% BSA (Thermo Fisher Scientific, Cat# B14),
122 2% normal goat serum (Thermo Fisher Scientific, Cat# 31872), in PBS) for 1 h. Second, non-
123 permeabilized fixed neurons were prepared by incubation with 4% (w/v) paraformaldehyde / 4%
124 (w/v) sucrose (Thermo Fisher Scientific, Cat# 28906, Fisher Scientific, Cat# BP-2201) at room

125 temperature (8 min) followed by incubation (1 h) in blocking buffer. Neurons prepared by both
126 methods were incubated overnight with primary antibodies to GluN1 (1:100, Millipore, Cat# 05-
127 432, RRID: AB_390129) and β -Tubulin (1:500), Covance Research Products Inc, Cat# PRB-
128 433C-200, RRID: AB_291636) in blocking buffer and then washed. The primary antibodies
129 were detected by incubation with anti-mouse or anti-rabbit Ig conjugated to Alexa Fluor 488 or
130 633 (1:200, Molecular Probes, Cat# A-11094, RRID: AB_221544; Thermo Fisher Scientific,
131 Cat# A21100, RRID: AB_10374307). DNA was detected by staining with DAPI (Vectashield
132 with DAPI, Vector Laboratories, Cat# H-1200). Fluorescence was visualized using a Leica TCS
133 SP2 confocal microscope equipped with a 405-nm diode laser. The mean fluorescence
134 intensity was quantitated using ImageJ software (RRID:SCR_001775).

135

136 **Preparation of synaptosomes**

137 Hippocampi from 4 mice (age 8-12 weeks) were isolated and homogenized in Syn-PER buffer
138 (Thermo Fisher Scientific, Cat# 87793). Briefly, neuronal tissue was homogenized in Syn-PER
139 reagent, centrifuged following manufacturer's instruction, followed by suspension of the resulting
140 synaptosome pellet in Syn-PER reagent to yield 3-4 μ g/ μ l of synaptic protein. The synaptosomes
141 contain the complete presynaptic terminal, including mitochondria and synaptic vesicles, and
142 also the postsynaptic membrane and the postsynaptic density (Villasana et al., 2006).

143

144 **RNA analysis**

145 The expression of mRNA was examined by quantitative RT-PCR analysis using a 7500 Fast
146 real-time PCR machine. Taqman® assays were used to quantitate *cFos* (Mm00487425_m1),
147 *cJun* (Mm00495062_s1), *Bdnf* (Mm00432069_m1), *GluN1* (*Grin1*, Mm00433800_m1), *GluN2A*
148 (*Grin2a*, Mm00433802_m1) and *GluN2B* (*Grin2b*, Mm00433820_m1) (Thermo Fisher
149 Scientific). The relative mRNA expression was normalized by measurement of *Gapdh*
150 (4352339E-0904021; Thermo Fisher Scientific) in each sample using Taqman® assays.

151

152

153 **Immunoblot analysis**

154 Tissue extracts were prepared from snap-frozen brain regions from JIP1^{WT} and JIP1^{TA} adult
155 mice (8-12 week-old) using Triton lysis buffer (20 mM Tris-pH 7.4, 1% Triton-X100, 10%
156 glycerol, 137 mM NaCl, 2 mM EDTA, 25 mM β -glycerophosphate, 1 μ M sodium orthovanadate,
157 1 μ M PMSF, 10 μ g/mL Leupeptin, and 10 μ g/mL Aprotinin). Extracts (20-50 μ g of protein) were
158 examined by protein immunoblot analysis by probing with antibodies to pSer⁶³-cJun (1:1000,
159 Cell Signaling Technologies Cat# 2361, RRID: AB_490908), JNK (1:1000, Cell Signaling
160 Technologies Cat# 9252, RRID: AB_2250373), GAPDH (Cell Signaling Technologies Cat#
161 2118, RRID: AB_561053, GluN2B (1:1000, Cell Signaling Technologies Cat#4212S, RRID:
162 AB_2112463), SAP102 (1:1000, Cell Signaling Technologies Cat# 3730S, RRID: AB_2092180),
163 pERK1/2 (1:1000, Cell Signaling Technologies Cat# 5683P, RRID: AB_10841299), pSer¹³³
164 CREB (1:1000, Cell Signaling Technologies Cat# 9198, RRID: AB_2561044) and CREB
165 (1:1000, Cell Signaling Technologies Cat#9197, RRID: AB_321277), ERK2 (1:1000, Santa Cruz
166 Biotechnology Cat# sc-81457, RRID: AB_1122619), JNK1/2 (Santa Cruz Biotechnology Cat#
167 sc-137019, RRID: AB_2140722), pJNK (Santa Cruz Biotechnology Cat# sc-6254, RRID:
168 AB_628232) and GluN2A (1:500, Millipore Cat# 07-632, RRID: AB_310837), pY¹⁴⁷² GluN2B
169 (1:1000, Millipore Cat# AB5403, RRID: AB_11210694; GluN1 (Millipore Cat# 05-432, RRID:
170 AB390129), GluA1 (1:2000, Millipore Cat# 04-855, RRID: AB_1977216), GluA2 (1:1000,
171 Millipore Cat# 07-261, RRID: AB_2116167), Synapsin I (1:1000, Millipore Cat# AB 1543, RRID:
172 AB_11210367), β -Tubulin (1:5000, Covance Research Products Inc Cat# PRB-435P-100,
173 RRID: AB_291637), PSD-95 (1:2000, Sigma-Aldrich Cat# P246, RRID: AB_260911) and KIF17
174 (1:1000, Sigma-Aldrich Cat# K3638, RRID: AB_477148). Immunocomplexes were detected by
175 fluorescence using anti-mouse (1:5000, LI-COR Biosciences Cat# 926-32210, RRID:

176 AB_621842) and anti-rabbit secondary IRDye antibodies, (1:5000, LI-COR Biosciences Cat#
177 827-08365, RRID: 10796098) and quantitated using a LI-COR Imaging system.

178

179 **Multiplexed ELISA**

180 Quantitative analysis of pSer⁶³-cJun (Bio-Rad, Cat#171-V50003M), cJun (Bio-Rad, Cat#171-
181 V60002M), pJNK (Bio-Rad, Cat#171-V50011M), JNK (Bio-Rad, Cat#171-V60007M), pERK
182 (Bio-Rad, Cat#171-V50006M) and ERK1/2 (Bio-Rad, Cat#171-V60003M) was performed using
183 Bio-Plex Pro Cell Signaling Reagent kit (Bio-Rad, Cat#171-304006M) and a Luminex 200
184 instrument (Millipore-Sigma).

185

186 **Kainate-induced excitotoxicity**

187 JIP1^{WT} and JIP1^{TA} mice (8-12 week-old) were injected intraperitoneally with 30 mg/kg kainic acid
188 (Tocris, Cat# 0222) (Yang et al., 1997). At 2h post-treatment, the mice were perfused with 4%
189 paraformaldehyde. Brains were harvested and fixed for an additional 24h in 4%
190 paraformaldehyde, then dehydrated and embedded in paraffin. Coronal sections (5 μ m) were
191 cut, rehydrated and subjected to heat-induced antigen retrieval (Vector Laboratories, cat# H-
192 3301). Sections were blocked for 1h at room temperature (1% BSA, 2% normal goat serum,
193 0.4% Triton-X100 in PBS) and incubated overnight with primary antibodies to pSer⁶³-cJun
194 (1:100, Cell Signaling Technologies Cat# 2361, RRID: AB_490908), or cFos (1:200, Cell
195 Signaling Technologies Cat# 4384S, RRID: AB_10698737) or cJun (1:100, Santa Cruz
196 Biotechnology Biotechnology Cat# sc-1694, RRID:AB_631263). The primary antibodies were
197 detected by incubation with anti-rabbit Ig conjugated to Alexa Fluor 488 (1:200, Thermo Fisher
198 Scientific Cat# A11008, RRID: AB_143165). DNA was detected by staining with DAPI
199 (Vectashield with DAPI, Vector Laboratories, Cat# H-1200). Fluorescence was visualized using
200 a Leica TCS SP2 confocal microscope equipped with a 405-nm diode laser.

201

202 **Surgery and infusions**

203 Mice were anesthetized with 1.2% Avertin (2, 2, 2-Tribromoethanol, Sigma-Aldrich, #T4, 840-2,
204 15.5 ml tert-amyl alcohol (2-methyl-2-butanol), Fisher, #A730-1) and implanted bilaterally with
205 26 gauge guide cannulae (Plastics One) into the dorsal hippocampus (anteroposterior (AP) - 0.5
206 mm, lateral 1 mm, depth 1.3 mm). Mice were allowed to recover for at least 7 days prior to
207 behavioral experiments. Intrahippocampal infusions were made using custom 28 gauge
208 injectors (Plastics One, Cat# C232I/SPC) that extended 1 mm beyond the tips of the guide
209 cannulae. On the day of the experiment, bilateral injections were performed using an infusion
210 pump (CMA/100, CMA/Microdialysis) at a constant rate of 0.5 μ l/min (final volume: 0.25 μ l/side).
211 The competitive NMDA receptor antagonist, D,L-2-amino-5-phosphonovaleric acid (APV; 10
212 μ g/ml; Sigma, Cat# A5282), was dissolved in artificial cerebrospinal fluid (aCSF) (130 mM NaCl,
213 3.5 mM KCl, 10 mM glucose, 1.25 mM NaH_2PO_4 , 2.0 mM CaCl_2 , 1.5 mM MgSO_4 and 24 mM
214 NaHCO_3). Controls received equal volumes of aCSF infused at the same rate. All infusions
215 were made 15 minutes before contextual fear conditioning.

216

217 **Analysis of dendritic spine density and morphology**

218 Golgi staining was performed using the FD Rapid Golgi Stain Kit (FD Neurotechnologies, Cat#
219 PK401) following the manufacturer's guidelines. Coronal sections (150 μ m) were obtained
220 using a microtome (Leica VT1000S). Spines examined were apical (*stratum radiatum*) and
221 basal (*stratum oriens*) dendrites of CA1 pyramidal neurons. CA1 pyramidal neurons were
222 traced using a Zeiss Axioskop 2 Plus microscope with a 100x oil immersion objective. Only
223 pyramidal neurons that exhibited complete impregnation and not obscured by other neurons or
224 artifacts were examined. Five neurons per animal were three-dimensionally reconstructed using
225 NeuroLucida Software (MicroBrightField) (RRID:SCR_001775). At least three apical (>50 μ m
226 from soma) and three basal (>30 μ m from soma) dendritic segments (>25 μ m length) were

227 quantified in each neuron. Spine densities were calculated as mean numbers of spines per 10
228 μm per dendrite per neuron in individual mice. Dendritic arborization was carried out using a
229 Sholl analysis of the apical and basilar dendrites of these neurons. Briefly, a series of
230 increasingly large concentric circles centered at the cell body and separated by 10 μm radius
231 intervals were superimposed upon traces of apical and basilar dendrites; the number of
232 dendritic intersections with each concentric circle was recorded. On the basis of morphology,
233 spines were classified into the following categories: thin, mushroom, and stubby (Korobova and
234 Svitkina, 2010).

235

236 **Analysis of tissue sections**

237 Paraformaldehyde-fixed brains were cryoprotected in 30% sucrose in 0.1 M PBS for 48 h at
238 4°C. Immunohistochemical analysis was performed on free-floating sections cut at 30 μm on a
239 cryostat. The sections were washed once with PBS and blocked with 5% goat serum (Vector
240 Laboratories, Cat# S-1000) in PBST (PBS + 0.3% Triton X-100) for 1 h. The sections were then
241 incubated overnight with primary antibodies to JIP1 (1:500, BD Biosciences, Cat# 611890,
242 RRID: AB_399370), anti-NeuN antibody (1:500, Millipore, Cat# MAB377, RRID: AB_2298772),
243 MAP2 antibody (1: 500, Millipore, Cat# AB5622, RRID: AB_91939), GAD67 antibody (1: 5000,
244 Millipore, Cat# MAB5406 RRID: AB_2278725), or GFAP antibody (1:150, Promega, Cat#
245 G5601, RRID:AB_430855) at 4°C. The sections were washed in PBST and incubated (1h) with
246 anti-mouse Ig or anti-rabbit Ig conjugated to Alexa Fluor 488 (Thermo Fisher Scientific Cat#
247 S11223 RRID: AB_2336881) or 546 (Thermo Fisher Scientific Cat# S11225 RRID:
248 AB_2532130). Nuclei were stained using DAPI (Vectashield with DAPI, Vector Laboratories,
249 Cat# H-1200). Images were obtained with a Zeiss Axio Imager 2 microscope at 10X and 20X
250 magnification. The mean fluorescence intensity was quantitated using ImageJ (RRID:
251 SCR_003070) software. Sections were also examined using Nissl stain (Thermo Fisher
252 Scientific, Cat# N21479).

253

254 **Fear conditioning and extinction**

255 Context-dependent and tone-dependent fear conditioning were performed using a computer-
256 controlled fear conditioning system (TSE, Bad Homburg, Germany) (Todorovic et al., 2007).
257 The fear conditioning was performed in a Plexiglas cage (36 x 21 x 20 cm) within a fear
258 conditioning box. The training (conditioning) consisted of a single trial. The mouse was exposed
259 to the conditioning context (180 s), followed by a tone [conditioned stimulus (CS), 30 s, 10 kHz,
260 75 dB SPL, pulsed 5 Hz]. After termination of the tone, a foot shock [unconditioned stimulus
261 (US), 0.8 mA or 0.4 mA, 2 s, constant current] was delivered through a stainless steel grid floor.
262 Under these conditions, the context served as background stimulus. Background contextual fear
263 conditioning but not foreground contextual fear conditioning, in which the tone is omitted during
264 training, has been shown to involve the hippocampus (Phillips and LeDoux, 1992). A
265 loudspeaker provided constant background noise. Contextual memory was tested in the fear-
266 conditioning box for 180 s without CS or US presentation (with background noise), 24 h after
267 contextual fear conditioning. The context-dependent extinction trials were performed at 24 h
268 intervals and consisted of non-reinforced, 3-min exposures (absence of a foot shock) to the
269 same context. For fear response extinction, the aforementioned protocol was used to acquire
270 contextual fear memory. Tone-dependent memory test was performed in a novel context
271 (context 2), 24 h after cued fear conditioning. Context 2 represented an identically sized cage
272 with a plain floor in a light-surrounding environment (350-500 lux) outside the fear-conditioning
273 box. No background noise was provided in context 2. During tone-dependent memory test, a
274 180-s pause without stimulation (pre-CS phase) preceded a 180-s period of auditory stimulation.
275 Freezing, defined as a lack of movement except for respiration was recorded every 10 sec by a
276 trained observer for a total of 18 sampling intervals. The mean number of observations
277 indicating freezing was expressed as a percentage of the total number of observations. The
278 exploration of the fear conditioning box during the training and activity burst produced by electric

279 foot-shock were automatically detected by an infrared beam system and analyzed using TSE
280 software.

281

282 **Morris water maze**

283 The water maze paradigm (Morris et al., 1982) was performed in a circular tank (diameter 180
284 cm; height 75 cm). It was located in a room with various distal cues. The tank was filled with
285 water (40 cm depth) maintained at 23°C, which was made opaque by the addition of a nontoxic
286 white paint. Inside the pool was a removable, circular (12 cm in diameter) Plexiglas platform 0.5
287 cm below the surface of the water. On the first two days, each mouse received visible platform
288 training that consisted of four consecutive trials of climbing onto the visible platform (with a black
289 plastic brick placed above it) until each subject was able to climb without help. For the hidden
290 platform task, the mice were given four consecutive trials per day starting from four different
291 pseudo-randomized start locations, with a 15 min inter-trial interval. Mice were allowed to
292 search for the hidden platform for 60 s. If the mice did not find the platform within 60 s, they
293 were guided to it. Mice were allowed to rest on the platform for 15 s after each trial. The hidden
294 platform task was composed of two phases: (1) 10 days (acquisition phase-days 3-13) with a
295 hidden platform in located in the center of the target quadrant; (2) reversal phase (day 14) with
296 the hidden platform located in the center of the quadrant opposite to the original target quadrant.
297 Reversal platform training was conducted without changing any distal visual cues. Probe trials
298 in which the escape platform was removed from the pool were conducted on days 10 (target
299 quadrant), 13 (target quadrant), and 15 (opposite quadrant). During the memory test (probe
300 trials), the platform was removed from the tank, and the mice were allowed to swim in the maze
301 for 60 s. The swimming path of the mice was recorded by a video camera and analyzed with the
302 computer-based tracking software Videomot 2 (TSE Systems, RRID:SCR_014334). The
303 percentage of swim distance spent in the platform quadrant and the latency to find the platform
304 were analyzed.

305

306 Rotarod test

307 Motor coordination and skill learning were assessed using an accelerating Rotarod (Stoelting).

308 Starting speed for the Rotarod began at 4 rpm and increased to 40 rpm over a 5-min period.

309 Mice were tested 4 times daily for 2 consecutive days with an inter-trial interval of 1 h between

310 tests. The latency to fall off the rod was measured for each trial.

311

312 Elevated plus maze test

313 The elevated plus-maze test for anxiety-related behaviors was performed as previously

314 described (Todorovic et al., 2007). Briefly, mice were placed in the center platform of the

315 elevated plus maze and allowed to explore for 5 min. Animal behavior was recorded by a video

316 camera connected to a PC and analyzed by videotracking software (VideoMot 2, TSE Systems,

317 RRID:SCR_014334). The percentage of time spent in the open and closed arms were

318 recorded. Shift of preference from the open to the closed arms was interpreted as an increase

319 of anxiety-like behavior. Locomotor activity was determined with this test by the distance

320 traveled.

321

322 Open field test

323 General exploratory activity and anxiety were assessed in an open field test. Mice were placed

324 in the center of an open field apparatus (50 x 50 cm) protected with 10 cm high opaque walls

325 and allowed to explore for 5 min. The field was divided into 16 equal squares (12.5 cm x 12.5

326 cm), consisting of 12 outer squares and 4 inner squares. Animal behavior was recorded by a

327 video camera connected to a PC and analyzed by videotracking software (VideoMot 2, TSE

328 Systems, RRID:SCR_014334). The amount of time spent in the inner and outer squares and

329 the total distance traveled was measured.

330

331

332 Acoustic startle and prepulse inhibition

333 Acoustic startle and prepulse inhibition test were performed as previously described (Pitts et al.,
334 2012). Mice were placed in the startle chamber (Responder-X, Columbus Instruments) and
335 allowed a 5 min acclimation period with the background noise (70 dB) continuously present.

336 Following the acclimation period, two blocks of trials were administered to assess the acoustic
337 startle response and prepulse inhibition, respectively. The first block of trials consisted of 8 sets
338 of 4 types of trials that were randomly distributed. Startle stimuli (40 ms) of varying intensities
339 were administered, with an interstimulus interval of 15 s. The stimulus intensities were 80, 90,
340 100, and 110 dB. Baseline activity was assessed by a set of no-stimulus trials. The startle
341 amplitude was defined as the peak response during a 100 ms sampling window beginning with
342 the onset of the startle stimulus. Mean startle amplitudes were derived by subtracting the
343 average startle amplitudes of stimulus intensities employed (80–110 dB) from the no-stimulus
344 trial (70 dB). The second block of trials consisted of 8 sets of 5 trial types, distributed randomly
345 and separated by 20 s interstimulus intervals. The trial types were (1) no-stimulus/background
346 noise (70 dB); (2) 40 ms, 110 dB startle alone; (3–5) 110 dB startle preceded 100 ms by one of
347 three 20 ms prepulses at the following intensities: 74, 80, 86 dB. The startle amplitude for each
348 subject at each of the different prepulse intensities was calculated using the following formula:
349 prepulse inhibition (PPI)=100–100×[response amplitude for prepulse stimulus paired with startle
350 stimulus/response amplitude for startle stimulus alone].

351

352 Electrophysiology

353 Extracellular recordings were performed as described previously (Lawrence et al., 2014).
354 Hippocampi of wild-type or mutant mice (8-12 weeks) were rapidly removed and briefly chilled in
355 ice-cold artificial CSF (aCSF) (consisting of the following: 130 mM NaCl, 3.5 mM KCl, 10 mM
356 glucose, 1.25 mM NaH₂PO₄, 2.0 mM CaCl₂, 1.5 mM MgSO₄ and 24 mM NaHCO₃ (equilibrated

357 with 95% O₂/5% CO₂, pH 7.4). Transverse slices 350 μm thick were prepared with a Vibratome
358 (Leica; VT1200S) and maintained at least 1 h in a holding chamber containing aCSF. The
359 slices were then transferred to a recording chamber and perfused (3 mL/min) with aCSF at
360 32°C. CA1 field EPSPs (fEPSPs) were recorded with a glass electrode filled with 3 M NaCl
361 (resistance 1-1.5 MΩ) by stimulating the Schaffer collateral fibers through a bipolar stimulating
362 electrode. The slope of the initial rising phase (20–60% of the peak amplitude) of the fEPSP
363 was used as a measure of the postsynaptic response. Basal synaptic neurotransmission was
364 studied by plotting stimulus strength or fiber volley against fEPSP slope to generate input–
365 output relationships. Paired-pulse facilitation (PPF) was defined as the second fEPSP slope
366 divided by the first at various inter-stimulus intervals (10, 50, 90, 130, 170, 210 and 250 ms).
367 For the LTP and long-term depression (LTD) measurements a minimum of 20 min of baseline
368 stimulation (0.05 Hz) was recorded every minute at an intensity that evoked a response 40% of
369 the maximum response. The strong tetanic LTP induction protocol consisted of two 100-Hz
370 tetani (1 s each), with an interval of 20 s between tetani. The weak LTP induction protocol
371 consisted of 900 pulses given at 10-Hz. To induce NMDA receptor-dependent LTD, a 1-Hz and
372 0.5-Hz single pulse stimuli were delivered for 15 and 30 min, respectively (900 stimuli). To
373 induce mGluR-dependent LTD, slices were incubated with 100 μM (S) –3,5-
374 dihydroxyphenylglycine (DHPG) (Tocris, Cat# 0805) for 5 min. For the depotentiation study LTP
375 was evoked by HFS with two trains of 100 Hz (20 s between tetani). Ten minutes after LTP
376 induction, depotentiation was induced by low frequency stimulation consisting of 900 pulses
377 delivered at 1 Hz for 15 min. fEPSP responses were recorded using a computer with WinLTP
378 data acquisition software (WinLTP Ltd, Bristol, UK). For pharmacological studies, JNK-in-8
379 (Selleckchem, Cat# S 4901) (6μM in aCSF with 10% DMSO) or vehicle were applied for 20 min
380 prior to testing and were maintained throughout the recording period.

381 For excitatory post-synaptic current (EPSC) measurements, mice (6 – 10 weeks old)
382 were anesthetized with isoflurane (Sigma Aldrich, Cat# 792632) and perfused with ice cold

383 sucrose solution containing: 200 mM sucrose, 20 mM glucose, 5 mM KCl, 1.2 mM NaH₂PO₄, 25
384 mM NaHCO₃, 0.5 mM CaCl₂, 7 mM MgCl₂, 1.3 mM ascorbic acid and 2.4 mM sodium pyruvate.
385 Transverse sections (350 μm) of the hippocampus were made and then incubated in aCSF at
386 34°C (20 min) before storing at room temperature. The aCSF for these experiments was
387 composed of: 125 mM NaCl, 10 mM glucose, 2.8 mM KCl, 1 mM NaH₂PO₄, 26 mM NaHCO₃, 2
388 mM CaCl₂, 1.5 mM MgSO₄. Whole-cell voltage clamp recordings were done at 32°C utilizing an
389 EPC-10 amplifier and Patchmaster acquisition software (HEKA Instruments Inc., Bellmore, NY,
390 RRID: SCR_000034). Data acquisition and analysis was performed on a MacPro computer
391 (Apple Inc., Cupertino, CA). Bicuculline (30 μM) (Tocris, Cat# 0130) and CGP-55845 (1 μM)
392 (Tocris, Cat# 1248) were added to the artificial aCSF to block GABA_A and GABA_B responses,
393 respectfully. Both sucrose and artificial CSF solutions were continually bubbled with
394 95%O₂/5%CO₂. Patch pipettes were filled with an intracellular solution containing: 130 mM Cs-
395 gluconate, 5 mM NaCl, 0.5 mM CaCl₂, 2 mM MgCl₂, 10 mM HEPES, 5 mM Cs₄BAPTA, 2 mM
396 MgATP, 0.3 mM Na₂GTP. The intracellular solution was titrated to pH 7.2 and 280 mOsm. CA1
397 principal cells were held at either -70 or +50 mV to measure the AMPA and NMDA receptor
398 components of EPSCs, respectively. Stimulation of the Schaffer collaterals synapsing onto the
399 CA1 cells was performed using an A360 stimulus isolation unit (World Precision Instruments,
400 Sarasota, FL) with a monopolar platinum iridium electrode placed in the *stratum radiatum*
401 approximately 350 μm from the cell body. The stimulation intensity was adjusted to be
402 approximately 75% of the threshold for firing an action potential. Peak amplitudes were
403 analyzed utilizing Igor Pro v.6.3 (RRID: SCR000325).

404

405 **Experimental design and statistical analysis**

406 Data were statistically analyzed using StatView (SAS Institute, Cary, NC) and GraphPad
407 Prism 6 software (GraphPad, San Diego, CA). Student's t-test was used for comparing two
408 conditions, and ANOVA was used with Bonferroni post hoc test for comparing more than two

409 conditions. All data are expressed as means \pm SEM. The accepted level of significance was
410 $p \leq 0.05$, indicated by an asterisk; p values ≤ 0.01 are indicated by double asterisks, while p
411 values ≤ 0.001 are indicated by triple asterisks.
412

413 Results

414 The aim of this study was to examine the impact of JIP1-regulated JNK activation on neuronal
415 function and behavior. To accomplish this aim we generated a novel mouse model harboring a
416 T103A point mutation in the *Jip1* gene (also known as *Mapk8ip1*). These mutant
417 *Mapk8ip1*^{T103A/T103A} mice (JIP1^{TA}) exhibit a profound defect in JIP1-mediated JNK activation
418 compared to control JIP1^{WT} animals. We therefore used this mutant mouse to determine the
419 contribution of JIP1-mediated JNK activation to NMDA-dependent receptor signaling, memory
420 and synaptic plasticity.

421 JIP1 expression in hippocampal neurons

422 Our initial studies were designed to examine the expression of JIP1 protein in the hippocampus.
423 Immunohistochemical staining of tissue sections demonstrated that JIP1 is expressed in the
424 CA1, CA3, and the dentate gyrus (DG) regions of the hippocampus (**Fig. 1A**). JIP1 was
425 primarily found on dendrites (colocalization with MAP2) and to a lesser extent on cell bodies
426 (colocalization with NeuN) of the CA1/CA3 pyramidal and DG granule neurons (**Fig. 1A**).

427 We next examined the hippocampal architecture of JIP1^{TA} and JIP1^{WT} mice. Qualitative
428 analysis of Nissl- (**Fig. 1 B,C**) and Golgi-stained (**Fig. 2A**) coronal sections did not reveal
429 differences in hippocampus morphology between JIP1^{TA} and JIP1^{WT} mice. Moreover, analysis
430 of basal and apical dendrites from Golgi-stained CA1 pyramidal neurons revealed no significant
431 differences in dendritic branching, spine density, or spine type (**Fig. 2A-E**). In addition, the
432 intensity and distribution of the neuronal marker NeuN ($t_{(6)} = 0.89$, $p=0.41$; two-tailed unpaired
433 Student's t-test), the dendritic marker MAP2 ($t_{(6)} = 0.71$, $p=0.51$; two-tailed unpaired Student's t-
434 test), the GABAergic interneuron marker GAD67 ($t_{(6)} = 0.27$, $p=0.79$; two-tailed unpaired
435 Student's t-test), and the glial marker GFAP ($t_{(6)} = 0.44$, $p=0.67$; two-tailed unpaired Student's t-
436 test), were similar in JIP1^{TA} and JIP1^{WT} mice (**Fig. 1B-D**). Collectively, these data indicate that

437 the Thr¹⁰³Ala mutation in JIP1 did not cause detectable changes in basic hippocampus
438 morphology.

439 ***JIP1-mediated JNK activation in the hippocampus***

440 We have previously demonstrated that JIP1^{TA} mice exhibit defects in metabolic stress-induced
441 JNK activation in adipose tissue (Morel et al., 2010). To test whether the Thr¹⁰³Ala mutation in
442 JIP1 also caused defects in JNK activation in neural tissue, we examined a model of JIP1-
443 dependent JNK activation (kainate excitotoxicity) in the hippocampus. Examination of the DG
444 following short-term exposure to kainate caused JIP1-dependent JNK activation and
445 phosphorylation of the JNK substrate cJun and JIP1-independent increased expression of cJun
446 and cFos (Whitmarsh et al., 2001). We found that kainate caused a similar increase in cJun
447 and cFos expression in JIP1^{TA} and JIP1^{WT} mice (**Fig. 3B,C**). In contrast, kainate caused
448 increased cJun phosphorylation in JIP1^{WT}, but not JIP1^{TA} mice (**Fig. 3A**). These data
449 demonstrate that the Thr¹⁰³Ala mutation suppresses JIP1-mediated JNK activation in the
450 hippocampus. Time-course analysis confirmed that cJun phosphorylation in the hippocampus
451 of kainate-stimulated JIP1^{WT} mice was strongly suppressed in JIP1^{TA} mice after exposure to
452 kainate (two-way ANOVA: genotype $F_{(1,32)} = 15.11$, $p < 0.001$; time $F_{(3,32)} = 34.26$, $p < 0.001$;
453 genotype x time $F_{(3,32)} = 5.05$, $p = 0.005$) (**Fig. 3D,E**). These data extend our previous finding that
454 JIP1^{TA} mice exhibit defects in JIP1-dependent JNK activation in adipose tissue (Morel et al.,
455 2010) to demonstrate that JIP1^{TA} mice also exhibit profound defects in JIP1-mediated JNK
456 activation in the hippocampus.

457 To test how JIP1-mediated JNK activation contributes to a physiologically relevant
458 response, we examined the effect of contextual fear conditioning, which was previously shown
459 to cause transient JNK activation in the dorsal hippocampus (Sherrin et al., 2010). Immunoblot
460 analysis using antibodies to JNK and phospho-JNK was performed to assess changes in JNK
461 activation in dorsal hippocampal extracts from JIP1^{WT} and JIP1^{TA} mice that were subjected to

462 single-trial contextual fear conditioning. Extracts were prepared at various times following the
463 single-trial to correspond to the consolidation phase of contextual fear (Igaz et al., 2002). JNK
464 immunoblot analysis detects the 46 kDa (JNK1 α 1 & JNK1 β 1) and 54 kDa isoforms (JNK2 α 2,
465 JNK2 β 2, and JNK3 α 2) in brain (Davis, 2000). We found that contextual fear conditioning
466 caused an increase in 46-kDa phospho-JNK in JIP1^{WT} mice at 30 min (176 \pm 12% of naïve
467 control mice; Bonferroni post hoc test, $p < 0.001$) and 60 min (127 \pm 8% of naïve; Bonferroni post
468 hoc test, $p = 0.09$) (**Fig. 4**). In contrast, we found that JIP1^{TA} mice exhibited decreased 46-kDa
469 phospho-JNK at 30 min (75 \pm 11% of naïve; Bonferroni post hoc test, $p = 0.011$), 60 min (53 \pm
470 7% of naïve; $p < 0.001$) and 180 min (79 \pm 6% of naïve; $p = 0.009$) after contextual fear
471 conditioning (two-way ANOVA: genotype $F_{(1,50)} = 15.11$, $p < 0.001$; time $F_{(4,50)} = 10.42$, $p < 0.001$;
472 genotype x time $F_{(4,50)} = 22.11$, $p < 0.001$) (**Fig. 4**). These data demonstrate that the JIP1
473 Thr¹⁰³Ala mutation suppresses JNK activation caused by contextual fear conditioning.

474

475 *JIP1-mediated JNK activation suppresses NMDA-dependent synaptic plasticity*

476 JNK activation is associated with mechanistic changes in synaptic plasticity in the hippocampus
477 (Wang et al., 2004; Chen et al., 2005; Zhu et al., 2005; Li et al., 2007; Yang et al., 2011).
478 Consequently, synaptic plasticity may be altered by JIP1-dependent JNK activation in the
479 context of fear conditioning (**Fig. 4**). We therefore examined synaptic transmission in JIP1^{WT}
480 and JIP1^{TA} mice.

481 Basal synaptic transmission at Schaffer collateral-CA1 synapses in JIP1^{WT} and JIP1^{TA}
482 mice was characterized through the input-output (I/O) relationship of field excitatory
483 postsynaptic potentials (fEPSPs). Analysis revealed that the fEPSP slopes, plotted against the
484 stimulation strength, were comparable in slices from JIP1^{WT} and JIP1^{TA} mice (two-way repeated
485 measures ANOVA: genotype $F_{(1,420)} = 0.23$, $p = 0.63$; amplitude $F_{(14,442)} = 79.27$, $p < 0.001$;
486 genotype x amplitude $F_{(14,420)} = 0.35$, $p = 0.63$) (**Fig. 5A**). Similarly, when the fEPSPs slopes were

487 plotted as a function of increasing fiber volley amplitudes, no differences between JIP1^{WT} and
488 JIP1^{TA} mice were detected (**Fig. 5B**). Moreover, paired-pulse facilitation, indicative of
489 presynaptic plasticity (Zucker and Regehr, 2002), at Schaffer collateral-CA1 synapses from
490 JIP1^{TA} mice was similar to JIP1^{WT} mice at several inter-pulse intervals (two-way repeated
491 measures ANOVA: genotype $F_{(1,223)} = 0.08$, $p = 0.78$); interval $F_{(6,223)} = 13.56$, $p < 0.001$; genotype
492 x interval $F_{(8,208)} = 0.15$, $p = 0.98$) (**Fig. 5C**). These data demonstrate similar basal synaptic
493 transmission in the hippocampi of JIP1^{TA} and JIP1^{WT} mice.

494 To determine whether the JIP1 Thr¹⁰³Ala mutation affects NMDA receptor-dependent
495 forms of synaptic plasticity (Citri and Malenka, 2008), LTP was measured using a high-
496 frequency tetanic stimulation protocol (HFS: 2 trains of 1 sec 100-Hz, separated by 20 sec).
497 Similar potentiation was produced in both JIP1^{WT} and JIP1^{TA} mice (**Fig. 5D**; fEPSPs were
498 potentiated to $145 \pm 7\%$ for JIP1^{WT} and $146 \pm 4\%$ for JIP1^{TA}) ($t_{(18)} = 0.12$, $p = 0.89$; two-tailed
499 unpaired Student's t-test), indicating that the ability to induce LTP with strong stimulation was
500 unimpaired in JIP1^{TA} mice. We next examined whether the threshold stimulation for induction of
501 LTP (Hu et al., 2007) differed between JIP1^{WT} and JIP1^{TA} mice. A 900-pulse train of 10 Hz
502 stimulation resulted in a modest, but detectable, degree of LTP in slices obtained from JIP1^{TA}
503 mice (**Fig. 5E**; $122 \pm 4\%$ of baseline at 50-60 min after LTP induction), though with minimal
504 post-tetanic potentiation, whereas fEPSPs in JIP1^{WT} slices were not potentiated (**Fig. 5E**; $92.1 \pm$
505 5.5% of baseline) ($t_{(18)} = 7.61$, $p < 0.001$; two-tailed unpaired Student's t-test), with a trend toward
506 depression. These data demonstrate that LTP could be induced at lower frequencies in JIP1^{TA}
507 mice compared with JIP1^{WT} mice.

508 We also examined the induction of NMDA receptor-dependent LTD (Collingridge et al.,
509 2010) in JIP1^{WT} and JIP1^{TA} mice. We found that low-frequency stimulation (LFS), consisting of
510 900 single pulses at 1 Hz for 15 min, generated robust LTD in JIP1^{WT} mice, but LTD was absent
511 in JIP1^{TA} mice (**Fig. 5F**) (JIP1^{WT} mice, $72 \pm 2\%$; JIP1^{TA} mice, $98 \pm 3\%$; $p < 0.01$) ($t_{(18)} = 7.05$,
512 $p < 0.001$; two-tailed unpaired Student's t-test). In view of the similar post-tetanic depression

513 [initial dip] between JIP1^{WT} and JIP1^{TA} brain slices, we determined whether JIP1^{TA} mice exhibit
514 other forms of LTD. We therefore induced LTD by delivering the same number of single pulses
515 (900) at 0.5 Hz for 30 min (**Fig. 5G**). This form of LTD also relies on NMDA receptors (Dudek
516 and Bear, 1992), but depends to a greater degree on release of calcium from intracellular stores
517 (Nakano et al., 2004). This LTD protocol produced equivalent depression in both JIP1^{TA} and
518 JIP1^{WT} mice (**Fig. 5G**; JIP1^{WT}, 68% ± 3%; JIP1^{TA}, 66% ± 2%) ($t_{(26)} = 0.55$, $p=0.58$; two-tailed
519 unpaired Student's t-test). These data indicate that disruption of JIP1-mediated JNK activation
520 reduces the optimal frequency stimulation for LTD, while enabling LTP at lower stimulation
521 frequencies at Schaffer collateral-CA1 synapses (**Fig. 5H**).

522 Two different forms of LTD coexist at Schaffer collateral-CA1 synapses in the
523 hippocampus, one dependent on NMDA receptors and another dependent on the activity of
524 metabotropic glutamate receptors (mGluRs), specifically mGluR5 (Huber et al., 2001). Thus, we
525 next examined a possible effect of the JIP1^{TA} mutation on mGluR-dependent LTD. We found
526 that a 5-min bath application of 100 μM DHPG (a group I mGluR agonist) to acute slices
527 resulted in a persistent depression of Schaffer collateral-evoked responses that was
528 comparable between JIP1^{TA} and JIP1^{WT} slices (**Fig. 5I**; 62% ± 1% of baseline at 60 min post-
529 drug application for JIP1^{TA} versus 65% ± 8% for JIP1^{WT}) ($t_{(18)} = 0.68$, $p=0.49$; two-tailed unpaired
530 Student's t-test). These results suggest that whereas the JIP1^{TA} mutation blocks the NMDAR-
531 dependent forms of LTD, it does not affect the mGluR-dependent form.

532 Another important aspect of synaptic modification is synaptic depotentiation, namely that
533 the synaptic potentiation could be subsequently reversed by LFS. In view of the finding that two
534 trains of HFS at 100 Hz induced significant LTP in response to a 20-s inter-tetanus interval in
535 both groups of mice (**Fig. 5J**), we used this HFS protocol followed by LFS 10 min later (900
536 pulses at 1 Hz) to induce depotentiation. One hour after the LFS, the evoked responses in both
537 JIP1^{WT} and JIP1^{TA} mice dropped to the baseline level (100% ± 4% compared with baseline

538 before the HFS for JIP1^{WT}, and 101% ± 3% for JIP1^{TA}) ($t_{(18)} = 0.23$, $p=0.82$; two-tailed unpaired
539 Student's t-test), indicating effective LFS-induced depotentiation in both genotypes.

540 We next tested whether application of a selective inhibitor of JNK would mimic effects of
541 the JIP1 Thr¹⁰³Ala mutation on NMDA-receptor dependent forms of LTP and LTD. Slices were
542 obtained from wild-type mice and exposed either to the selective JNK inhibitor JNK-in-8 (6 μM)
543 or solvent (aCSF) for 20 min prior to stimulation protocols. The drug application was maintained
544 throughout the recording period. Basal synaptic transmission was not affected by JNK-in-8 as
545 indicated by the unchanged input–output relation (two-way repeated measures ANOVA:
546 genotype $F_{(1,308)} = 0.88$, $p= 0.35$); amplitude $F_{(14,308)} = 61.73$, $p<0.001$; genotype x amplitude
547 $F_{(14,308)} = 0.35$, $p=0.63$) and unchanged paired-pulse facilitation (two-way repeated measures
548 ANOVA: genotype $F_{(1,132)} = 0.46$, $p= 0.56$); interval $F_{(6,132)} = 42.12$, $p<0.001$; genotype x interval
549 $F_{(6,132)} = 1.17$, $p=0.11$) (**Fig. 6A, B**). In addition, inhibiting JNK activation in slices did not affect
550 HFS LTP (**Fig. 6C**, 60 min after 2X100Hz tetanization: 127 ± 6% of baseline for vehicle-treated
551 slices vs. 125 ± 5% for JNK-in-8-treated slices) ($t_{(22)} = 0.25$, $p=0.81$; two-tailed unpaired
552 Student's t-test). However, JNK inhibition prevented the induction of LTD using the 1 Hz
553 stimulation protocol (**Fig. 6D** - vehicle-treated slices, 77 ± 3%; JNK-in-8-treated slices, 101 ±
554 4%; $p<0.05$) ($t_{(18)} = 4.81$, $p<0.001$; two-tailed unpaired Student's t-test). The latter result closely
555 parallels the result obtained for the JIP1^{TA} slices (cf. **Fig. 5F**). Thus, these data confirm that
556 JIP1-mediated JNK activation plays an essential, but differential, role in certain forms NMDA-
557 receptor dependent synaptic plasticity.

558

559 ***JIP1^{TA} mice exhibit increased NMDA receptor signaling***

560 It is established that JIP scaffold proteins influence NMDA receptor activity (Kennedy et al.,
561 2007). The induction of synaptic plasticity at lower stimulation frequencies detected in JIP1^{TA}
562 mice compared with JIP1^{WT} mice (**Fig. 6**) may therefore be mediated by changes in NMDA
563 receptor signaling. Indeed, we found increased expression of NMDA receptor subunits GluN1

564 ($t_{(8)} = 2.66$, $p=0.029$; two-tailed unpaired Student's t-test), GluN2A ($t_{(8)} = 2.85$, $p=0.037$; two-
565 tailed unpaired Student's t-test), and GluN2B proteins ($t_{(8)} = 2.65$, $p=0.027$; two-tailed unpaired
566 Student's t-test) (but not *mRNA*) in the whole hippocampus of JIP1^{TA} mice compared to JIP1^{WT}
567 mice (**Fig. 7A-C**). Control studies detected no differences in the expression of the AMPA
568 receptor subunits GluA1 and GluA2 (**Fig. 7A**). The increased expression of NMDA receptor
569 subunits was also detected in hippocampal synaptoneurosome (Fig. 7D) and by increased cell
570 surface detection of GluN1 by immunofluorescence analysis of hippocampal neurons ($t_{(16)} =$
571 2.85 , $p=0.012$; two-tailed unpaired Student's t-test), (**Fig. 7E,F**) cultured from JIP1^{TA} mice
572 compared with JIP1^{WT} mice. These changes were associated with biochemical evidence of
573 increased NMDA receptor activity through assessment of downstream signaling changes,
574 including increased GluN2B Tyr¹⁴⁷² phosphorylation (Salter and Kalia, 2004) (**Fig. 7A**),
575 increased *cFos* mRNA expression ($t_{(9)} = 3.31$, $p=0.009$; two-tailed unpaired Student's t-test),
576 (Bading et al., 1993) (**Fig. 7G**), ERK phosphorylation ($t_{(8)} = 3.11$, $p=0.017$; two-tailed unpaired
577 Student's t-test) (Xia et al., 1996) (**Fig. 7H**), and CREB phosphorylation ($t_{(8)} = 5.25$, $p=0.008$;
578 two-tailed unpaired Student's t-test) (Ginty et al., 1993) (**Fig. 7H**). Control experiments
579 demonstrated that the expression of KIF17, a microtubule motor that transports GluN2B
580 vesicles and regulates synaptic plasticity (Yin et al., 2011; Yin et al., 2012), was similar in
581 JIP1^{WT} and JIP1^{TA} mice (**Fig. 7H**). Together, these data indicate that JIP1^{TA} mice may exhibit
582 increased NMDA receptor signaling in the hippocampus compared with JIP1^{WT} mice.

583 To functionally test whether NMDA receptor signaling was increased in JIP1^{TA} mice
584 compared with JIP1^{WT} mice, we examined excitatory post-synaptic currents (EPSCs) via whole-
585 cell recordings of CA1 pyramidal cells in acute hippocampus slices. For CA1 pyramidal cells
586 held under voltage clamp at -70 mV, the response to Schaffer collateral stimulation is primarily
587 mediated by AMPA receptors. The NMDA receptor-mediated component of EPSCs is readily
588 distinguished from the AMPA receptor component by measuring current responses at a
589 membrane potential of +50 mV approximately 30 ms after stimulation when approximately 90%

590 of the AMPA receptor response has decayed (Liao et al., 1995; Myme et al., 2003). We found
591 that the average NMDA receptor-mediated peak EPSC was 1.6-fold larger in JIP1^{TA} mice
592 compared with JIP1^{WT} mice ($t_{(31)} = 2.41$, $p=0.022$; two-tailed unpaired Student's t-test) (**Fig.**
593 **8A,B**), while the average peak amplitude of the AMPA receptor-mediated EPSCs were similar in
594 JIP1^{TA} and JIP1^{WT} mice ($t_{(31)} = 0.28$, $p=0.77$; two-tailed unpaired Student's t-test) (**Fig. 8A,C**).
595 These findings were reflected in the NMDA/AMPA peak current ratio calculated for each cell
596 tested. JIP1^{WT} mice had a NMDA/AMPA receptor ratio of $37 \pm 4\%$, whereas JIP1^{TA} mice yielded
597 a significantly larger ratio of $50 \pm 4\%$ ($t_{(31)} = 2.21$, $p=0.038$; two-tailed unpaired Student's t-test)
598 (**Fig. 8D**). This analysis demonstrated that NMDA receptor signaling is increased in JIP1^{TA}
599 hippocampal neurons compared with those of JIP1^{WT} mice. To confirm this conclusion, we
600 examined NMDA receptor-stimulated gene expression in primary JIP1^{TA} and JIP1^{WT}
601 hippocampal neurons. We found that NMDA-induced expression of *brain-derived neurotrophic*
602 *factor (Bdnf)* mRNA (Ghosh et al., 1994; Tabuchi et al., 2000) and *cFos* mRNA (Bading et al.,
603 1993; Xia et al., 1996) by JIP1^{TA} neurons were increased when compared with JIP1^{WT} neurons
604 ([two-way ANOVA: genotype $F_{(1,29)} = 70.26$, $p<0.001$; time $F_{(2,29)} = 39.7$, $p<0.001$; genotype x time
605 $F_{(2,29)} = 14.91$, $p<0.001$; for *Bdnf* mRNA]; [two-way ANOVA: genotype $F_{(1,30)} = 17.67$, $p<0.001$;
606 time $F_{(2,30)} = 182.1$, $p<0.001$; genotype x time $F_{(2,30)} = 7.98$, $p<0.001$; for *cFos* mRNA]) (**Fig.**
607 **8E,F**). Together, these data indicate that the increased NMDA-mediated signaling detected in
608 the JIP1^{TA} hippocampus is due to enhanced NMDA receptor activity in individual neurons.

609

610 ***JIP1-mediated JNK activation in locomotor, sensory and emotional responses***

611 To address the possibility that increased NMDA receptor signaling in JIP1^{TA} mice compared
612 with JIP1^{WT} mice may cause behavioral changes, we first performed a battery of basic
613 behavioral tests of CNS function on JIP1^{WT} and JIP1^{TA} mice. We found that anxiety-related
614 behavior was increased in JIP1^{TA} mice. For example, JIP1^{TA} mice in an elevated plus maze
615 spent less time in the open arms, compared with JIP1^{WT} mice ($t_{(18)} = 2.79$, $p= 0.012$; two-tailed

616 unpaired Student's t-test), with no changes in locomotor activity ($t_{(18)} = 0.76$, $p = 0.45$; two-tailed
617 unpaired Student's t-test) (**Fig. 9, A-C**). Moreover, JIP1^{TA} mice spent significantly less time in
618 the center ($t_{(18)} = 5.40$, $p < 0.001$; two-tailed unpaired Student's t-test) and more in the periphery
619 ($t_{(18)} = 6.46$, $p < 0.001$; two-tailed unpaired Student's t-test) during an open field test compared to
620 JIP1^{WT} animals (**Fig. 9, D-E**). Consistent with previous reports (Grillon et al., 1998), elevated
621 anxiety in JIP1^{TA} mice was accompanied by an enhancement of the startle response to strong
622 acoustic stimuli (two-way repeated measures ANOVA: genotype $F_{(1,42)} = 5.42$, $p = 0.035$; stimulus
623 $F_{(3,42)} = 105.42$, $p < 0.001$; genotype x stimulus = 9.25, $p < 0.001$) (**Fig. 9F**). No changes in
624 sensorimotor gating (pre-pulse inhibition) were observed (two-way repeated measures ANOVA:
625 genotype $F_{(1,28)} = 0.13$, $p = 0.722$) (**Fig. 9G**). We also found that "fast" improvement in motor
626 coordination on the accelerating Rotarod was comparable between JIP1^{WT} and JIP1^{TA} mice.
627 However, during the second day of Rotarod training JIP1^{TA} mice did not display improved "slow"
628 skill learning, unlike JIP1^{WT} mice, as indicated by significant genotype x trial interaction value
629 (two-way repeated measures ANOVA: genotype $F_{(1,98)} = 4.84$, $p = 0.045$), trial $F_{(7,98)} = 7.73$,
630 $p < 0.001$; genotype x trial $F_{(7,98)} = 3.34$, $p = 0.003$) (**Fig. 9H**). Taken together, these data
631 demonstrate that JIP1^{TA} mice have normal sensory and motor activity, and attention function.
632 However, JIP1^{TA} mice displayed increased levels of anxiety-related behaviors and altered skill
633 learning.

634 ***Improved extinction-resistant contextual fear memory in JIP1^{TA} mice***

635 Contextual fear conditioning triggers JIP1-dependent JNK activation in the hippocampus (**Fig.**
636 **4**). Moreover, JNK activation in the hippocampus is implicated in some forms of hippocampus-
637 dependent memory (Sherrin et al., 2011). We therefore compared JIP1^{WT} and JIP1^{TA} mice to
638 determine if JIP1-mediated JNK activation is required for the behavioral response to contextual
639 fear conditioning. The mice received either "weak" (0.4 mA shock) or "strong" (0.8 mA shock)
640 training and were then re-exposed to the chamber 24 h later to assess long-term fear memory

641 (Shalin et al., 2006). The two training procedures were employed to adjust for nociceptive
642 sensitivity and also to test whether a “weak” stimulation protocol, similar to one that facilitated
643 synaptic plasticity (cf. **Fig. 5E**), results in enhanced hippocampal memory in JIP1^{TA} mice. JIP1^{TA}
644 and JIP1^{WT} mice showed no differences in freezing or activity during the exploration period
645 before the foot-shock (data not shown), or after the 0.8mA foot-shock delivery ($t_{(19)} = 0.46$,
646 $p=0.65$; two-tailed unpaired Student’s t-test). (**Fig. 10A**, right panel). Significantly enhanced
647 contextual freezing of JIP1^{TA} mice compared with JIP1^{WT} controls was found 24 h after “strong”
648 training (**Fig. 10A**, left panel, mean percentage freezing: JIP1^{TA} = $85 \pm 3\%$; JIP1^{WT} = $59 \pm 4\%$)
649 ($t_{(19)} = 5.11$, $p<0.001$; two-tailed unpaired Student’s t-test). This enhancement of contextual fear
650 was more pronounced in JIP1^{TA} mice when the “weak” paradigm was used (**Fig. 10B**, mean
651 percentage freezing: JIP1^{TA} = $81 \pm 4\%$; JIP1^{WT} = $44 \pm 5\%$) ($t_{(26)} = 5.26$, $p<0.001$; two-tailed
652 unpaired Student’s t-test). We next investigated short-term memory by testing JIP1^{TA} and
653 JIP1^{WT} mice immediately or 1 hr after the “strong” conditioning paradigm. We found that JIP1^{TA}
654 and JIP1^{WT} mice displayed similar responses in the both contextual tests ($t_{(20)} = 0.18$, $p=0.85$; 0
655 hr post-conditioning, two-tailed unpaired Student’s t-test) ($t_{(26)} = 0.11$, $p= 0.75$; 1hr post-
656 conditioning, two-tailed unpaired Student’s t-test) (**Fig. 10A**, left panel). Thus, JIP1^{TA} and JIP1^{WT}
657 mice did not differ in exploration activity, nociceptive reaction to electric shock, post-shock
658 freezing response, or short-term fear memory. These findings also indicate that the increased
659 anxiety phenotype observed with the JIP1^{TA} mice does not appear to fundamentally affect
660 shock-induced and post-shock behaviors, including contextual fear conditioning and learning
661 (see also **Fig. 11**). Nevertheless, JIP1^{TA} mice exhibited increased long-term fear memory
662 compared with JIP1^{WT} mice (**Fig. 10A,B**).

663 We then tested whether contextual fear memory is differentially affected in JIP1^{TA} and
664 JIP1^{WT} mice following antagonism of the NMDA receptors. JIP1^{TA} and JIP1^{WT} mice were
665 implanted with cannulae into the dorsal hippocampus and subjected to contextual fear
666 conditioning. A selective NMDA receptor antagonist, D,L-2-amino-5-phosphonovaleric acid

667 (APV; 10 μ g/ml; 0.5 ml) or solvent (aCSF), was infused into the dorsal hippocampus (i.h.) 15
668 min prior to training. Both JIP1^{TA} and JIP1^{WT} mice given APV showed substantially reduced
669 freezing to context compared to mice that received aCSF prior to conditioning (two-way
670 ANOVA: genotype $F_{(1,36)} = 8.76$, $p = 0.0054$; treatment $F_{(1,36)} = 143.06$, $p < 0.001$; genotype x
671 treatment = 5.29, $p = 0.027$) (**Fig. 10C**). However, no differences between APV-treated JIP1^{TA}
672 mice and APV-treated JIP1^{WT} mice were observed (Bonferroni post hoc test: $p = 0.62$) (**Fig.**
673 **10C**), indicating that memory facilitating effects observed in JIP1^{TA} were mediated via activation
674 of NMDA receptors. Taken together, these experiments show that blockade of JIP1-mediated
675 JNK activation can improve contextual learning induced by a relatively mild learning protocol
676 and that enhanced NMDA receptor function is required for this facilitatory effect of JIP1^{TA}
677 mutation on learning.

678 Previous studies have demonstrated that activation of hippocampal NMDA receptor
679 regulates fear extinction (Szapiro et al., 2003; Suzuki et al., 2004; Leaderbrand et al., 2014),
680 and that NMDA receptor blockade can prevent fear extinction in a variety of fear-related tasks
681 (Santini et al., 2001; Sotres-Bayon et al., 2007). Thus, we extended our cognitive evaluation of
682 JIP1^{TA} mice by assessing contextual fear extinction to further assess the link of JIP1-JNK
683 activation through NMDA receptors. Conditioned JIP1^{TA} and JIP1^{WT} mice were subjected to
684 brief (3-min) daily extinction trials (E1-E7) by non-reinforced placement in the training context for
685 7 days after contextual conditioning. During the extinction trials, JIP1^{TA} mice exhibited almost
686 unchanged freezing responses, indicating nearly fully impaired extinction compared to JIP1^{WT}
687 mice (repeated measure ANOVA: genotype $F_{(1,108)} = 388.76$, $p < 0.001$; time $F_{(6,108)} = 36.26$, $p <$
688 0.001 ; $F_{(6,108)}$ genotype x time = 25.35, $p < 0.001$) (**Fig. 10D**). Overall, these results indicate that
689 the enhanced contextual fear observed in JIP1^{TA} mice is strongly resistant to extinction.

690 Finally, cue-dependent fear conditioning was assessed in JIP1^{TA} mice and JIP1^{WT}
691 controls. As with contextual fear conditioning, mice received either a “strong” or a “weak”
692 training protocol, both consisting of a single pairing of tone and shock at 0.8mA and 0.4mA,

693 respectively. In both protocols, JIP1^{TA} mice, compared to JIP1^{WT} controls, displayed significantly
694 more freezing when re-exposed to the tone 24 h post-training (**Fig. 10E**, left panel, mean
695 percentage freezing: “weak” cued test- JIP1^{TA} = 66 ± 3%; JIP1^{WT} = 44 ± 4%) ($t_{(20)} = 3.71$, $p=0.01$;
696 two-tailed unpaired Student's t-test) (**Fig. 10E**, right panel, mean percentage freezing: “strong”
697 cued test- JIP1^{TA} = 70 ± 3%; JIP1^{WT} = 55 ± 4%) ($t_{(20)} = 2.65$, $p=0.015$; two-tailed unpaired
698 Student's t-test), indicating that JIP1^{TA} mice display memory enhancement in the fear learning
699 tasks in a manner involving both amygdala- and hippocampus-dependent memory systems.

700

701 ***Improved spatial learning in JIP1^{TA} mice***

702 We next tested JIP1^{TA} and JIP1^{WT} mice using the Morris water maze (MWM) protocol, a
703 hippocampus-dependent spatial memory task (Morris et al., 1982). During the hippocampus-
704 independent visible portion of the training, both JIP1^{TA} and JIP1^{WT} mice readily learned to find
705 the marked platform (**Fig. 11A**). Mice were then trained to swim to a hidden platform located in
706 a fixed location of the pool (target quadrant, T, **Fig. 11A,D**). JIP1^{TA} mice had significantly
707 decreased escape latencies compared to JIP1^{WT} mice on days 6-9 and day 12 of training (two-
708 way repeated measures ANOVA: genotype $F_{(1,208)} = 11.03$, $p= 0.0049$); time $F_{(8,208)}= 21.01$,
709 $p<0.001$; genotype x time $F_{(8,208)}= 0.74$, $p=0.65$) (**Fig. 11A**). However, JIP1^{TA} and JIP1^{WT} mice
710 did not differ in the time spent in the platform-containing quadrant during probe trials on day 10
711 (**Fig. 11B**, 36 ± 3% of time in quadrant T for JIP1^{TA}; 35 ± 2% JIP1^{WT}) ($t_{(26)} = 0.27$, $p=0.783$; two-
712 tailed unpaired Student's t-test) and day 13 (**Fig. 11C**, 38 ± 5% of time in quadrant T for JIP1^{TA}
713 mice; 36 ± 3% JIP1^{WT} mice) ($t_{(26)} = 0.34$, $p=0.734$; two-tailed unpaired Student's t-test).

714 Although JIP1^{TA} mice did not display preference for the target quadrant during probe trials, the
715 decrease in escape latency during training suggests that the presence of the JIP1 Thr¹⁰³Ala
716 mutation appears to moderately affect gradual learning of the hidden platform water maze task.

717 To test whether JIP1^{TA} mice display enhanced fast spatial learning, we performed a
718 reversal of the hidden platform in the MWM. The hidden platform was moved to the opposite

719 quadrant of the pool (new target quadrant (NT)) and the mice were trained to swim to this new
720 location for four trials separated by 15-20 min (**Fig. 11D**). JIP1^{TA} mice learned significantly faster
721 to swim to the new platform location compared to control mice (two-way repeated measures
722 ANOVA: genotype $F_{(1,78)} = 16.37$, $p = 0.0012$; time $F_{(3,78)} = 1.98$, $p = 0.13$; genotype x time $F_{(3,78)} =$
723 1.86 , $p = 0.15$) (**Fig. 11E**). Moreover, the JIP1^{TA} mice displayed increased preference for the NT
724 quadrant during a probe trial given on probe day 15 (**Fig. 11F**; time spent in NT quadrant: $41 \pm$
725 2% for JIP1^{TA}; $23 \pm 4\%$ for JIP1^{WT}) ($t_{(26)} = 4.02$, $p < 0.001$; two-tailed unpaired Student's t-test).
726 This enhancement in spatial reversal learning of the new platform location was accompanied by
727 a decrease in the percent of time JIP1^{TA} mice spent searching for the platform in the previously
728 correct quadrant (O) ($t_{(26)} = 2.34$, $p = 0.028$; two-tailed unpaired Student's t-test) (**Fig. 11F**).
729 These data indicate that the Thr¹⁰³Ala mutation in JIP1 allows for improved fast spatial learning.

730 ***JNK binding is required for JIP1-mediated NMDA receptor regulation of learning and***
731 ***memory***

732 To confirm that JIP1-mediated JNK activation plays a critical role in NMDA receptor-dependent,
733 hippocampus-dependent learning and memory, we tested an independent mouse model of
734 defective JIP1-mediated JNK activation: JIP1 lacking the JNK binding domain (JBD). To create
735 a mouse model lacking the JBD of JIP1 (JIP1^{ΔJBD} mice), the core of the JBD (Leu¹⁶⁰-Asn¹⁶¹-
736 Leu¹⁶²) mediating a hydrophobic interaction of JIP1 with JNK (Whitmarsh et al., 2001; Heo et al.,
737 2004) was replaced with Gly¹⁶⁰-Arg¹⁶¹-Gly¹⁶² in JIP1^{ΔJBD} mice (**Fig. 12A-B**). Immunoblot analysis
738 of brain extracts from JIP1^{WT} and JIP1^{ΔJBD} mice indicated similar levels of JIP1 protein
739 expression (**Fig. 12C**). To establish that the ΔJBD mutation blocks JIP1-mediated JNK
740 activation *in vivo*, we compared kainate-induced excitotoxicity in the hippocampus of JIP1^{WT} and
741 JIP1^{ΔJBD} mice. This analysis demonstrated that kainate caused similar increases in cJun
742 expression in the dentate gyrus of JIP1^{WT} and JIP1^{ΔJBD} mice, but kainate-stimulated cJun
743 phosphorylation was markedly suppressed in JIP1^{ΔJBD} mice compared with JIP1^{WT} mice (**Fig.**

744 **12D,E).** These data confirm that JIP1^{ΔJBD} mice represent a model of defective JIP1-mediated
745 JNK signaling.

746 We then examined contextual and cued fear conditioning to assess the effect of the
747 JIP1^{ΔJBD} mutation on learning and memory. The JIP1^{ΔJBD} mice displayed a significantly
748 increased conditioned freezing response in both learning tasks compared to the JIP1^{WT} mice
749 when tested at 24 hours after training (**Fig. 13A left panel:** mean percentage contextual
750 freezing; JIP1^{WT} = 58 ± 3%; JIP1^{ΔJBD} = 89 ± 3%; $t_{(18)} = 6.30$, $p < 0.001$; two-tailed unpaired
751 Student's t-test; **Fig. 13A right panel:** mean percentage cued freezing; JIP1^{WT} = 51 ± 1%;
752 JIP1^{ΔJBD} = 69 ± 6%; $t_{(20)} = 2.97$, $p = 0.007$; two-tailed unpaired Student's t-test), a result very
753 similar to that observed for the JIP1^{TA} mice (**Fig. 10**). JIP1^{ΔJBD} mice exhibited enhanced
754 learning in the MWM (two-way repeated measures ANOVA: genotype $F_{(1,162)} = 26.04$, $p < 0.001$);
755 time $F_{(8,162)} = 126.7$, $p < 0.001$; genotype x time $F_{(8,162)} = 1.75$, $p = 0.84$), and spent significantly more
756 time in the target quadrant compared to control JIP1^{WT} mice when subjected to probe trials on
757 day 9 ($t_{(18)} = 4.02$, $p < 0.001$) (**Fig. 13C**, left panel; 41 ± 2% of time in quadrant T for JIP1^{ΔJBD}; 32
758 ± 1% of time in quadrant T for JIP1^{WT}) and day 13 (**Fig. 13C**, right panel; 48 ± 4% of time in
759 quadrant T for JIP1^{ΔJBD}; 36 ± 3% of time in quadrant T for JIP1^{WT}) ($t_{(18)} = 2.44$, $p = 0.027$; two-
760 tailed unpaired Student's t-test). This was an unexpected finding, as JIP1^{TA} mice did not show
761 enhanced memory retention in the hidden platform MWM task (**cf. Fig. 11B, C**). The larger
762 phenotype in the JIP1^{ΔJBD} mice in the MWM compared to the JIP1^{TA} mice may result from a
763 greater effect of the JNK binding site mutation on JIP1-mediated JNK activation than the
764 mutation of the T103 phosphorylation site on JIP1.

765 We then examined reversal learning by moving the hidden platform to the opposite
766 quadrant (**Fig. 13D**, left panel). Similar to JIP1^{TA} mice, the JIP1^{ΔJBD} mice showed shorter
767 latencies than control mice in finding the new platform location during a one-day trial period
768 (data not shown). Moreover, JIP1^{ΔJBD} mice spent significantly more time in the new target
769 quadrant compared to JIP1^{WT} control mice (**Fig. 13D**, right panel; mean percentage of time

770 spent in new target quadrant [NT] was $49 \pm 3\%$, for JIP1^{ΔJBD}; $28 \pm 4\%$ for JIP1^{WT}) ($t_{(18)} = 4.21$,
771 $p < 0.001$; two-tailed unpaired Student's t-test). Furthermore, like JIP1^{TA} mice, we found
772 significantly increased expression of GluN1, GluN2A, and GluN2B in the hippocampus of
773 JIP1^{ΔJBD} mice as compared to hippocampi from JIP1^{WT} mice (**Fig. 13E**) and increased ERK
774 activation ($t_{(8)} = 2.57$, $p = 0.033$; two-tailed unpaired Student's t-test) (**Fig. 13F**).

775 Together, these analyses of JIP1^{TA} and JIP1^{ΔJBD} mice confirm that loss of JIP1-mediated
776 JNK activation enhances NMDA-dependent hippocampus-dependent memory.

777

778 **Discussion**

779 The JIP1 scaffold protein can assemble a functional JNK signaling module formed by members
780 of the mixed-lineage protein kinase family of MAP3K, the MAP2K family member MKK7, and
781 JNK (Whitmarsh et al., 1998). However, JIP1 also functions as an adapter protein that
782 mediates transport by microtubule motor proteins (Fu and Holzbaur, 2014), including kinesin-1
783 (Verhey et al., 2001; Whitmarsh et al., 2001) and dynein (Standen et al., 2009; Fu and
784 Holzbaur, 2013). These two functions of JIP1 compromise the interpretation of loss-of-function
785 studies focused on the analysis of JIP1 knockout mice (Whitmarsh et al., 2001; Kennedy et al.,
786 2007). To overcome this limitation, we studied two mouse models with germ-line mutations in
787 the *Jip1* gene that prevent JIP1-mediated JNK activation. First, a point mutation of the JIP1
788 phosphorylation site Thr¹⁰³ (by replacement with Ala) in JIP1^{TA} mice suppresses JIP1-mediated
789 JNK activation (**Fig. 3**) by disrupting the regulated interaction of mixed-lineage protein kinases
790 with JIP1 (Morel et al., 2010). Second, a three-residue mutation of the JIP1 site that binds JNK
791 in JIP1^{ΔJBD} mice prevents JIP1-mediated JNK activation (**Fig. 12**). These complementary
792 mouse models therefore provided an opportunity to selectively disrupt JIP1-mediated JNK
793 activation *in vivo*.

794 It is established that the JIP1 scaffold protein mediates JNK activation in the neuronal
795 response to excitotoxin (Whitmarsh et al., 2001) and in adipose tissue during metabolic stress
796 responses (Jaeschke et al., 2004; Morel et al., 2010). The results of the present study extend
797 these findings to neural functioning by demonstrating that JIP1-linked JNK activation in the
798 hippocampus regulates contextual fear conditioning in a NMDA receptor-dependent fashion.
799 This finding builds on the previous demonstration that JNK1-deficient mice exhibit enhanced
800 contextual fear conditioning (Sherrin et al., 2010) and altered synaptic plasticity (Li et al., 2007).

801 We further show that JIP1-mediated JNK activation regulates NMDA receptor signal
802 transduction associated with an altered threshold for LTP, decreased long-term fear memory,
803 and decreased spatial memory (**Figs. 5, 6, 8, 10, 11 & 13**). These observations are consistent
804 with the conclusion that JNK normally functions to negatively regulate mechanisms responsible
805 for learning and memory (Sherrin et al., 2011). We found that the enhanced learning in JIP1
806 mutant mice was associated with an increase in the NMDA receptor component of the synaptic
807 response, and enhanced activity of downstream pathways that facilitate induction of NMDA
808 receptor-dependent LTP. This is consistent with previous reports that have separately
809 implicated both JNK signaling (Sherrin et al., 2010) and CA1 hippocampal NMDA receptors in
810 contextual fear conditioning, spatial learning, and synaptic plasticity (Kutsuwada et al., 1996;
811 Tsien et al., 1996; Tang et al., 1999; Liu et al., 2004; Lau and Zukin, 2007; Yashiro and Philpot,
812 2008; Brigman et al., 2010). These data indicate that JIP1-mediated JNK activation may
813 constrain synaptic plasticity, learning and memory through attenuation of NMDA receptor
814 function. Furthermore, decreases in JIP1 level and/or localization affecting JNK activity, perhaps
815 resulting from distinct signaling pathways (e.g. glutamate-mediated down-regulation of JIP1
816 level in growth cones (Dajas-Bailador et al., 2014); Ca²⁺-dependent degradation of JIP1
817 (Allaman-Pillet et al., 2003), would thus be predicted to reduce this constraint, leading to
818 enhanced learning and memory.

819 The increased NMDA receptor signaling caused by loss of JIP1-mediated JNK activation
820 in JIP1^{TA} mice is associated with increased expression of the NMDA receptor subunits GluN2A
821 and GluN2B (**Fig. 7**). This increase in the levels of NMDA receptor subunits is significant
822 because it is established that changes in GluN2A and GluN2B expression cause altered
823 plasticity and memory (Tang et al., 1999; Brigman et al., 2010; Chao et al., 2013). This may be
824 mediated by extending the integration time window for NMDA receptor signaling coincident with
825 pre- and postsynaptic activity, and decreasing the threshold for inducing long-term synaptic

826 changes. Indeed, a constraint by JIP1-JNK on plasticity thresholds may, in turn, regulate
827 information processing and learning (Kiyama et al., 1998; Hawasli et al., 2007; Hu et al., 2007).
828 This is consistent with the observation that loss of JIP1-mediated JNK activation in JIP1^{TA} mice
829 enables the establishment of LTP at lower stimulation frequencies (**Fig. 5H**), with the converse
830 being a requirement for higher stimulation frequencies needed in the presence of JIP1-JNK
831 activation. The mechanism of JIP1-dependent regulation of NMDA receptor subunit expression
832 (**Fig. 7A,B**) remains to be determined and may include changes in NMDA receptor membrane
833 insertion, internalization, or lateral movement into synapses (**Fig 14**). Additionally, JIP1 may
834 regulate NMDA receptor subunit expression through a post-transcriptional mechanism (**Fig. 14**).
835 Indeed, it is known that GluN1, GluN2 and GluN2B protein expression can be regulated by
836 CPEB3 (Chao et al., 2013), that GluN2A protein expression can be regulated by CPEB1
837 (Udagawa et al., 2012; Swanger et al., 2013), and that GluN2B expression can be regulated by
838 a microRNA (Harraz et al., 2012). Strikingly, the learning and memory phenotypes of *Cpeb3*^{-/-}
839 mice associated with increased NMDA receptor expression (Chao et al., 2013) are similar to the
840 phenotypes of the mice with defects in JIP1 function studied in the present study (JIP1^{TA} and
841 JIP1^{ΔJBD} mice).

842 It is possible that increased expression of NMDA receptor subunits only partially
843 accounts for the learning and memory phenotypes of JIP1^{TA} and JIP1^{ΔJBD} mice. Indeed, it has
844 been shown that cFyn mediates phosphorylation of the NMDA receptor subunit GluN2B on
845 Y¹⁴⁷², resulting in increased NMDA receptor activity (Salter and Kalia, 2004) by attenuating
846 NMDA receptor internalization (Roche et al., 2001; Prybylowski et al., 2005), increasing the
847 proper localization of the GluN2B NMDA receptors at synapses (Nakazawa et al., 2006), and
848 enhancing GluN2B NMDA receptor-mediated currents at CA1 synapses (Yang et al., 2012). In
849 the present study, increased GluN2B Y¹⁴⁷² phosphorylation resulted from disruption of JIP1-
850 mediated JNK activation in JIP1^{TA} mice (**Fig. 7A**), also perhaps contributing to the observed

851 increase in NMDA receptor signaling. This change in GluN2B Y¹⁴⁷² phosphorylation may be
852 caused by JIP1-mediated recruitment of cFyn (Kennedy et al., 2007) or by JNK-mediated
853 recruitment of PSD-95/Fyn complex (Kim et al., 2007). Another potential contributing factor may
854 be the binding of JIP1 to LRP8, a protein that regulates NMDAR signaling (Stockinger et al.,
855 2000; Beffert et al., 2005). Finally, it is possible that JIP1-mediated interactions with the
856 exchange factors Ras-GRF1 and Tiam1 may contribute to increased NMDA receptor dependent
857 activation of the ERK pathway and activity-dependent actin remodeling critical for synaptic
858 plasticity and memory (Buchsbaum et al., 2002; Krapivinsky et al., 2003; Tolia et al., 2007).

859 Contextual-fear learning recruits both the hippocampus and amygdala, while cued-fear
860 learning relies on the amygdala (Phillips and LeDoux, 1992). JIP^{TA} and JIP1^{ΔJBD} mice displayed
861 enhancement in both contextual and cued fear conditioning (**Figs. 10, 13**). As such, these
862 learning enhancements suggest that JIP1-mediated JNK activation is also important in the
863 amygdala. Although JIP1 is expressed in amygdala (preliminary observations), JNK signaling
864 and the importance of JIP1 in the amygdala have yet to be thoroughly investigated. We
865 hypothesize that the observed contextual-learning enhancement is, at least, in part due to a lack
866 of hippocampal JIP1-mediated JNK signaling. Not only is signal transduction altered in this
867 region, but JIP^{TA} and JIP1^{ΔJBD} mice also demonstrate an improved spatial water maze memory,
868 which classically relies on the hippocampus.

869 Genetic anomalies on the JNK pathway have also been associated with a subset of
870 other psychiatric disorders (Coffey, 2014). However, the degree to which and the mechanism
871 by which JNK is involved is unknown. JIP1^{TA} mutant mice display a range of behaviors
872 including exaggerated fear responses to cues associated with the danger, difficulty suppressing
873 fear behavior even when these cues no longer predict danger, elevated acoustic startle
874 response, and anxiety-like behaviors that may represent rodent homologues of the symptoms
875 that are diagnostic for trauma- and stressor-related disorders, such as posttraumatic stress

876 disorder (PTSD) (Shalev et al., 2017). These responses may be regulated by JIP1-mediated
877 JNK signaling in the hippocampus, the amygdala, or in various cortical regions that interconnect
878 to form the neural circuits that promote adaptation to stress and fear conditioning. Interestingly,
879 we have shown that intrahippocampal infusion with a JNK inhibitor prevents stress-induced
880 changes in fear conditioning (Sherrin et al, 2010). Thus, it is possible that drugs that target
881 the function of JIP1 to positively regulate JNK activity or NMDA receptor function (Myers and
882 Davis, 2007; Feder et al., 2014; Ori et al., 2015; Mataix-Cols et al., 2017) may therefore be
883 useful for the treatment of PTSD or anxiety disorders marked by abnormal fear learning and
884 maladaptive processing of information related to threat. Our study provides a proof-of-concept
885 that validates this approach using a model organism. An exciting future possibility is the
886 application of this strategy to the treatment of human fear and anxiety.

887 Overall, the results of this study suggest that JNK activation caused by the JIP1 scaffold
888 protein constrains learning and memory in a NMDA receptor-dependent fashion. This role of
889 JIP1 starkly differs from the related protein JIP2 that acts to promote NMDA receptor signaling
890 by a JNK-independent mechanism (Kennedy et al., 2007). Our studies of JIP1 therefore
891 establish a role for the JIP1-JNK pathway in NMDA receptor-dependent regulation of memory
892 acquisition, consolidation, and retention.

893

894 **References**

- 895
896 Allaman-Pillet N, Storling J, Oberson A, Roduit R, Negri S, Sauser C, Nicod P, Beckmann JS,
897 Schorderet DF, Mandrup-Poulsen T, Bonny C (2003) Calcium- and proteasome-
898 dependent degradation of the JNK scaffold protein islet-brain 1. *J Biol Chem* 278:48720-
899 48726.
900
- 901 Bading H, Ginty DD, Greenberg ME (1993) Regulation of gene expression in hippocampal
902 neurons by distinct calcium signaling pathways. *Science* 260:181-186.
903
- 904 Baptista J, Mercer C, Prigmore E, Gribble SM, Carter NP, Maloney V, Thomas NS, Jacobs PA,
905 Crolla JA (2008) Breakpoint mapping and array CGH in translocations: comparison of a
906 phenotypically normal and an abnormal cohort. *Am J Human Genet* 82:927-936.
907
- 908 Beffert U, Weeber EJ, Durudas A, Qiu SF, Masiulis I, Sweatt JD, Li WP, Adelmann G, Frotscher
909 M, Hammer RE, Herz J (2005) Modulation of synaptic plasticity and memory by Reelin
910 involves differential splicing of the lipoprotein receptor Apoer2. *Neuron* 47:567-579.
911
- 912 Brigman JL, Wright T, Talani G, Prasad-Mulcare S, Jinde S, Seabold GK, Mathur P, Davis MI,
913 Bock R, Gustin RM, Colbran RJ, Alvarez VA, Nakazawa K, Delpire E, Lovinger DM,
914 Holmes A (2010) Loss of GluN2B-containing NMDA receptors in CA1 hippocampus and
915 cortex impairs long-term depression, reduces dendritic spine density, and disrupts
916 learning. *J Neurosci* 30:4590-4600.
917
- 918 Buchsbaum RJ, Connolly BA, Feig LA (2002) Interaction of Rac exchange factors Tiam1 and
919 Ras-GRF1 with a scaffold for the p38 mitogen-activated protein kinase cascade. *Mol*
920 *Cell Biol* 22:4073-4085.
921
- 922 Chao HW, Tsai LY, Lu YL, Lin PY, Huang WH, Chou HJ, Lu WH, Lin HC, Lee PT, Huang YS
923 (2013) Deletion of CPEB3 Enhances Hippocampus-Dependent Memory via Increasing
924 Expressions of PSD95 and NMDA Receptors. *J Neurosci* 33:17008-17022.
925
- 926 Chen JT, Lu DH, Chia CP, Ruan DY, Sabapathy K, Xiao ZC (2005) Impaired long-term
927 potentiation in c-Jun N-terminal kinase 2-deficient mice. *J Neurochem* 93:463-473.
928
- 929 Citri A, Malenka RC (2008) Synaptic plasticity: Multiple forms, functions, and mechanisms.
930 *Neuropsychopharmacol* 33:18-41.
931
- 932 Coffey ET (2014) Nuclear and cytosolic JNK signalling in neurons. *Nat Rev Neurosci* 15:285-
933 299.
934
- 935 Collingridge GL, Peineau S, Howland JG, Wang YT (2010) Long-term depression in the CNS.
936 *Nat Rev Neurosci* 11:459-473.
937
- 938 Curran BP, Murray HJ, O'Connor JJ (2003) A role for c-Jun N-terminal kinase in the inhibition of
939 long-term potentiation by interleukin-1beta and long-term depression in the rat dentate
940 gyrus in vitro. *Neuroscience* 118:347-357.
941
- 942 Dajas-Bailador F, Bantounas I, Jones EV, Whitmarsh AJ (2014) Regulation of axon growth by
943 the JIP1-AKT axis. *J Cell Sci* 127:230-239.

- 944
945 Davis RJ (2000) Signal transduction by the JNK group of MAP kinases. *Cell* 103:239-252.
946
- 947 de Anda FC, Rosario AL, Durak O, Tran T, Graff J, Meletis K, Rei D, Soda T, Madabhushi R,
948 Ginty DD, Kolodkin AL, Tsai LH (2012) Autism spectrum disorder susceptibility gene
949 TAOK2 affects basal dendrite formation in the neocortex. *Nat Neurosci* 15:1022-1031.
950
- 951 Dickens M, Rogers JS, Cavanagh J, Raitano A, Xia Z, Halpern JR, Greenberg ME, Sawyers CL,
952 Davis RJ (1997) A cytoplasmic inhibitor of the JNK signal transduction pathway. *Science*
953 277:693-696.
954
- 955 Dudek SM, Bear MF (1992) Homosynaptic long-term depression in area CA1 of hippocampus
956 and effects of N-methyl-D-aspartate receptor blockade. *Proc Natl Acad Sci U S A*
957 89:4363-4367.
958
- 959 Feder A, Parides MK, Murrrough JW, Perez AM, Morgan JE, Saxena S, Kirkwood K, Aan Het
960 Rot M, Lapidus KA, Wan LB, Iosifescu D, Charney DS (2014) Efficacy of intravenous
961 ketamine for treatment of chronic posttraumatic stress disorder: a randomized clinical
962 trial. *JAMA Psychiatry* 71:681-688.
963
- 964 Fu MM, Holzbaur EL (2013) JIP1 regulates the directionality of APP axonal transport by
965 coordinating kinesin and dynein motors. *J Cell Biol* 202:495-508.
966
- 967 Fu MM, Holzbaur EL (2014) Integrated regulation of motor-driven organelle transport by
968 scaffolding proteins. *Trends Cell Biol* 24:564-574.
969
- 970 Ghosh A, Carnahan J, Greenberg ME (1994) Requirement for BDNF in activity-dependent
971 survival of cortical neurons. *Science* 263:1618-1623.
972
- 973 Ginty DD, Kornhauser JM, Thompson MA, Bading H, Mayo KE, Takahashi JS, Greenberg ME
974 (1993) Regulation of CREB phosphorylation in the suprachiasmatic nucleus by light and
975 a circadian clock. *Science* 260:238-241.
976
- 977 Giza J, Urbanski MJ, Prestori F, Bandyopadhyay B, Yam A, Friedrich V, Kelley K, D'Angelo E,
978 Goldfarb M (2010) Behavioral and cerebellar transmission deficits in mice lacking the
979 autism-linked gene *islet brain-2*. *J Neurosci* 30:14805-14816.
980
- 981 Grillon C, Morgan CA, Davis M, Southwick SM (1998) Effects of experimental context and
982 explicit threat cues on acoustic startle in Vietnam veterans with posttraumatic stress
983 disorder. *Biol Psychiat* 44:1027-1036.
984
- 985 Harraz MM, Eacker SM, Wang XQ, Dawson TM, Dawson VL (2012) MicroRNA-223 is
986 neuroprotective by targeting glutamate receptors. *Proc Natl Acad Sci U S A* 109:18962-
987 18967.
988
- 989 Hawasli AH, Benavides DR, Nguyen C, Kansy JW, Hayashi K, Chambon P, Greengard P,
990 Powell CM, Cooper DC, Bibb JA (2007) Cyclin-dependent kinase 5 governs learning and
991 synaptic plasticity via control of NMDAR degradation. *Nat Neurosci* 10:880-886.
992
- 993 Heo YS, Kim SK, Seo CI, Kim YK, Sung BJ, Lee HS, Lee JI, Park SY, Kim JH, Hwang KY, Hyun
994 YL, Jeon YH, Ro S, Cho JM, Lee TG, Yang CH (2004) Structural basis for the selective

- 995 inhibition of JNK1 by the scaffolding protein JIP1 and SP600125. *EMBO J* 23:2185-
996 2195.
- 997
- 998 Hu HL, Real E, Takamiya K, Kang MG, Ledoux J, Huganir RL, Malinow R (2007) Emotion
999 enhances learning via norepinephrine regulation of AMPA-Receptor trafficking. *Cell*
1000 131:160-173.
- 1001
- 1002 Huber KM, Roder JC, Bear MF (2001) Chemical induction of mGluR5- and protein synthesis--
1003 dependent long-term depression in hippocampal area CA1. *J Neurophysiol* 86:321-325.
- 1004
- 1005 Igaz LM, Vianna MR, Medina JH, Izquierdo I (2002) Two time periods of hippocampal mRNA
1006 synthesis are required for memory consolidation of fear-motivated learning. *J Neurosci*
1007 22:6781-6789.
- 1008
- 1009 Inoue A, Sawatari E, Hisamoto N, Kitazono T, Teramoto T, Fujiwara M, Matsumoto K, Ishihara
1010 T (2013) Forgetting in *C. elegans* is accelerated by neuronal communication via the TIR-
1011 1/JNK-1 pathway. *Cell Rep* 3:808-819.
- 1012
- 1013 Jaeschke A, Czech MP, Davis RJ (2004) An essential role of the JIP1 scaffold protein for JNK
1014 activation in adipose tissue. *Genes Dev* 18:1976-1980.
- 1015
- 1016 Kant S, Standen CL, Morel C, Jung DY, Kim JK, Swat W, Flavell RA, Davis RJ (2017) A Protein
1017 Scaffold Coordinates SRC-Mediated JNK Activation in Response to Metabolic Stress.
1018 *Cell Rep* 20:2775-2783.
- 1019
- 1020 Kennedy NJ, Martin G, Ehrhardt AG, Cavanagh-Kyros J, Kuan CY, Rakic P, Flavell RA,
1021 Treisman SN, Davis RJ (2007) Requirement of JIP scaffold proteins for NMDA-
1022 mediated signal transduction. *Genes Dev* 21:2336-2346.
- 1023
- 1024 Kim MJ, Futai K, Jo J, Hayashi Y, Cho K, Sheng M (2007) Synaptic accumulation of PSD-95
1025 and synaptic function regulated by phosphorylation of serine-295 of PSD-95. *Neuron*
1026 56:488-502.
- 1027
- 1028 Kiyama Y, Manabe T, Sakimura K, Kawakami F, Mori H, Mishina M (1998) Increased thresholds
1029 for long-term potentiation and contextual learning in mice lacking the NMDA-type
1030 glutamate receptor epsilon1 subunit. *J Neurosci* 18:6704-6712.
- 1031
- 1032 Korobova F, Svitkina T (2010) Molecular architecture of synaptic actin cytoskeleton in
1033 hippocampal neurons reveals a mechanism of dendritic spine morphogenesis. *Mol Biol*
1034 *Cell* 21:165-176.
- 1035
- 1036 Krapivinsky G, Krapivinsky L, Manasian Y, Ivanov A, Tyzio R, Pellegrino C, Ben-Ari Y, Clapham
1037 DE, Medina I (2003) The NMDA receptor is coupled to the ERK pathway by a direct
1038 interaction between NR2B and RasGRF1. *Neuron* 40:775-784.
- 1039
- 1040 Kunde SA, Rademacher N, Tzschach A, Wiedersberg E, Ullmann R, Kalscheuer VM, Shoichet
1041 SA (2013) Characterisation of de novo MAPK10/JNK3 truncation mutations associated
1042 with cognitive disorders in two unrelated patients. *Human Genet* 132:461-471.
- 1043
- 1044 Kutsuwada T, Sakimura K, Manabe T, Takayama C, Katakura N, Kushiya E, Natsume R,
1045 Watanabe M, Inoue Y, Yagi T, Aizawa S, Arakawa M, Takahashi T, Nakamura Y, Mori

- 1046 H, Mishina M (1996) Impairment of suckling response, trigeminal neuronal pattern
1047 formation, and hippocampal LTD in NMDA receptor epsilon 2 subunit mutant mice.
1048 *Neuron* 16:333-344.
1049
- 1050 Lau CG, Zukin RS (2007) NMDA receptor trafficking in synaptic plasticity and neuropsychiatric
1051 disorders. *Nat Rev Neurosci* 8:413-426.
1052
- 1053 Lawrence JL, Tong M, Alfulaj N, Sherrin T, Contarino M, White MM, Bellinger FP, Todorovic C,
1054 Nichols RA (2014) Regulation of Presynaptic Ca²⁺, Synaptic Plasticity and Contextual
1055 Fear Conditioning by a N-terminal beta-Amyloid Fragment. *J Neurosci* 34:14210-14218.
1056
- 1057 Leaderbrand K, Corcoran KA, Radulovic J (2014) Co-activation of NR2A and NR2B subunits
1058 induces resistance to fear extinction. *Neurobiol Learn Mem* 113:35-40.
1059
- 1060 Li XM, Li CC, Yu SS, Chen JT, Sabapathy K, Ruan DY (2007) JNK1 contributes to metabotropic
1061 glutamate receptor-dependent long-term depression and short-term synaptic plasticity in
1062 the mice area hippocampal CA1. *Eur J Neurosci* 25:391-396.
1063
- 1064 Liao D, Hessler NA, Malinow R (1995) Activation of postsynaptically silent synapses during
1065 pairing-induced LTP in CA1 region of hippocampal slice. *Nature* 375:400-404.
1066
- 1067 Liu L, Wong TP, Pozza MF, Lingenhoehl K, Wang Y, Sheng M, Auberson YP, Wang YT (2004)
1068 Role of NMDA receptor subtypes in governing the direction of hippocampal synaptic
1069 plasticity. *Science* 304:1021-1024.
1070
- 1071 Mataix-Cols D et al. (2017) D-Cycloserine Augmentation of Exposure-Based Cognitive Behavior
1072 Therapy for Anxiety, Obsessive-Compulsive, and Posttraumatic Stress Disorders: A
1073 Systematic Review and Meta-analysis of Individual Participant Data. *JAMA Psychiatry*
1074 74:501-510.
1075
- 1076 Morel C, Standen CL, Jung DY, Gray S, Ong H, Flavell RA, Kim JK, Davis RJ (2010)
1077 Requirement of JIP1-Mediated c-Jun N-Terminal Kinase Activation for Obesity-Induced
1078 Insulin Resistance. *Mol Cell Biol* 30:4616-4625.
1079
- 1080 Morris RG, Garrud P, Rawlins JN, O'Keefe J (1982) Place navigation impaired in rats with
1081 hippocampal lesions. *Nature* 297:681-683.
1082
- 1083 Morrison DK, Davis RJ (2003) Regulation of MAP kinase signaling modules by scaffold proteins
1084 in mammals. *Annu Rev Cell Dev Biol* 19:91-118.
1085
- 1086 Mukherjee PK, DeCoster MA, Campbell FZ, Davis RJ, Bazan NG (1999) Glutamate receptor
1087 signaling interplay modulates stress-sensitive mitogen-activated protein kinases and
1088 neuronal cell death. *J Biol Chem* 274:6493-6498.
1089
- 1090 Myers KM, Davis M (2007) Mechanisms of fear extinction. *Mol Psychiatry* 12:120-150.
1091
- 1092 Myme CIO, Sugino K, Turrigiano GG, Nelson SB (2003) The NMDA-to-AMPA ratio at synapses
1093 onto layer 2/3 pyramidal neurons is conserved across prefrontal and visual cortices. *J*
1094 *Neurophysiol* 90:771-779.
1095

- 1096 Nakano M, Yamada S, Udagawa R, Kato N (2004) Frequency-dependent requirement for
1097 calcium store-operated mechanisms in induction of homosynaptic long-term depression
1098 at hippocampus CA1 synapses. *Eur J Neurosci* 19:2881-2887.
1099
- 1100 Nakazawa T, Komai S, Watabe AM, Kiyama Y, Fukaya M, Arima-Yoshida F, Horai R, Sudo K,
1101 Ebine K, Delawary M, Goto J, Umemori H, Tezuka T, Iwakura Y, Watanabe M,
1102 Yamamoto T, Manabe T (2006) NR2B tyrosine phosphorylation modulates fear learning
1103 as well as amygdaloid synaptic plasticity. *EMBO J* 25:2867-2877.
1104
- 1105 Nihalani D, Wong HN, Holzman LB (2003) Recruitment of JNK to JIP1 and JNK-dependent JIP1
1106 phosphorylation regulates JNK module dynamics and activation. *J Biol Chem*
1107 278:28694-28702.
1108
- 1109 Ori R, Amos T, Bergman H, Soares-Weiser K, Ipser JC, Stein DJ (2015) Augmentation of
1110 cognitive and behavioural therapies (CBT) with d-cycloserine for anxiety and related
1111 disorders. *Cochrane Database Syst Rev*:CD007803.
1112
- 1113 Pellet JB, Haefliger JA, Staple JK, Widmann C, Welker E, Hirling H, Bonny C, Nicod P, Catsicas
1114 S, Waeber G, Riederer BM (2000) Spatial, temporal and subcellular localization of islet-
1115 brain 1 (IB1), a homologue of JIP-1, in mouse brain. *Eur J Neurosci* 12:621-632.
1116
- 1117 Phillips RG, LeDoux JE (1992) Differential contribution of amygdala and hippocampus to cued
1118 and contextual fear conditioning. *Behav Neurosci* 106:274-285.
1119
- 1120 Pitts MW, Raman AV, Hashimoto AC, Todorovic C, Nichols RA, Berry MJ (2012) Deletion of
1121 selenoprotein P results in impaired function of parvalbumin interneurons and alterations
1122 in fear learning and sensorimotor gating. *Neuroscience* 208:58-68.
1123
- 1124 Prybylowski K, Chang K, Sans N, Kan LL, Vicini S, Wenthold RJ (2005) The synaptic
1125 localization of NR2B-containing NMDA receptors is controlled by interactions with PDZ
1126 proteins and AP-2. *Neuron* 47:845-857.
1127
- 1128 Roche KW, Standley S, McCallum J, Ly CD, Ehlers MD, Wenthold RJ (2001) Molecular
1129 determinants of NMDA receptor internalization. *Nat Neurosci* 4:794-802.
1130
- 1131 Salter MW, Kalia LV (2004) SRC kinases: A hub for NMDA receptor regulation. *Rev Neurosci*
1132 5:317-328.
1133
- 1134 Santini E, Muller RU, Quirk GJ (2001) Consolidation of extinction learning involves transfer from
1135 NMDA-independent to NMDA-dependent memory. *J Neurosci* 21:9009-9017.
1136
- 1137 Shalev A, Liberzon I, Marmar C (2017) Post-Traumatic Stress Disorder. *N Engl J Med*
1138 376:2459-2469.
1139
- 1140 Shalin SC, Hernandez CM, Dougherty MK, Morrison DK, Sweatt JD (2006) Kinase suppressor
1141 of Ras1 compartmentalizes hippocampal signal transduction and subserves synaptic
1142 plasticity and memory formation. *Neuron* 50:765-779.
1143
- 1144 Sherrin T, Blank T, Todorovic C (2011) c-Jun N-terminal kinases in memory and synaptic
1145 plasticity. *Rev Neurosci* 22:403-410.
1146

- 1147 Sherrin T, Blank T, Hippel C, Rayner M, Davis RJ, Todorovic C (2010) Hippocampal c-Jun-N-
1148 terminal kinases serve as negative regulators of associative learning. *J. Neurosci*
1149 30:13348-13361.
1150
- 1151 Shoichet SA, Duprez L, Hagens O, Waetzig V, Menzel C, Herdegen T, Schweiger S, Dan B,
1152 Vamos E, Ropers HH, Kalscheuer VM (2006) Truncation of the CNS-expressed JNK3 in
1153 a patient with a severe developmental epileptic encephalopathy. *Human Genet* 118:559-
1154 567.
1155
- 1156 Sotres-Bayon F, Bush DE, LeDoux JE (2007) Acquisition of fear extinction requires activation of
1157 NR2B-containing NMDA receptors in the lateral amygdala. *Neuropsychopharmacol*
1158 32:1929-1940.
1159
- 1160 Standen CL, Kennedy NJ, Flavell RA, Davis RJ (2009) Signal transduction cross talk mediated
1161 by Jun N-terminal kinase-interacting protein and insulin receptor substrate scaffold
1162 protein complexes. *Mol Cell Biol* 29:4831-4840.
1163
- 1164 Stockinger W, Brandes C, Fasching D, Hermann M, Gotthardt M, Herz J, Schneider WJ, Nimpf
1165 J (2000) The reelin receptor ApoER2 recruits JNK-interacting proteins-1 and -2. *J Biol*
1166 *Chem* 275:25625-25632.
1167
- 1168 Suzuki A, Josselyn SA, Frankland PW, Masushige S, Silva AJ, Kida S (2004) Memory
1169 reconsolidation and extinction have distinct temporal and biochemical signatures. *J*
1170 *Neurosci* 24:4787–4795.
1171
- 1172 Swanger SA, He YA, Richter JD, Bassell GJ (2013) Dendritic GluN2A Synthesis Mediates
1173 Activity-Induced NMDA Receptor Insertion. *J. Neurosci* 33:8898-8908.
1174
- 1175 Szapiro G, Vianna MR, McGaugh JL, Medina JH, Izquierdo I (2003) The role of NMDA
1176 glutamate receptors, PKA, MAPK, and CAMKII in the hippocampus in extinction of
1177 conditioned fear. *Hippocampus* 13:53-58.
1178
- 1179 Tabuchi A, Nakaoka R, Amano K, Yukimine M, Andoh T, Kuraishi Y, Tsuda M (2000)
1180 Differential activation of brain-derived neurotrophic factor gene promoters I and III by
1181 Ca²⁺ signals evoked via L-type voltage-dependent and N-methyl-D-aspartate receptor
1182 Ca²⁺ channels. *J Biol Chem* 275:17269-17275.
1183
- 1184 Tang YP, Shimizu E, Dube GR, Rampon C, Kerchner GA, Zhuo M, Liu G, Tsien JZ (1999)
1185 Genetic enhancement of learning and memory in mice. *Nature* 401:63-69.
1186
- 1187 Todorovic C, Radulovic J, Jahn O, Radulovic M, Sherrin T, Hippel C, Spiess J (2007)
1188 Differential activation of CRF receptor subtypes removes stress-induced memory deficit
1189 and anxiety. *Eur J Neurosci* 25:3385-3397.
1190
- 1191 Tolias KF, Bikoff JB, Kane CG, Tolias CS, Hu L, Greenberg ME (2007) The Rac1 guanine
1192 nucleotide exchange factor Tiam1 mediates EphB receptor-dependent dendritic spine
1193 development. *Proc Natl Acad Sci U S A* 104:7265-7270.
1194
- 1195 Tsien JZ, Huerta PT, Tonegawa S (1996) The essential role of hippocampal CA1 NMDA
1196 receptor-dependent synaptic plasticity in spatial memory. *Cell* 87:1327-1338.
1197

- 1198 Udagawa T, Swanger SA, Takeuchi K, Kim JH, Nalavadi V, Shin J, Lorenz LJ, Zukin RS,
1199 Bassell GJ, Richter JD (2012) Bidirectional Control of mRNA Translation and Synaptic
1200 Plasticity by the Cytoplasmic Polyadenylation Complex. *Mol Cell* 47:253-266.
1201
- 1202 Verhey KJ, Meyer D, Deehan R, Blenis J, Schnapp BJ, Rapoport TA, Margolis B (2001) Cargo
1203 of kinesin identified as JIP scaffolding proteins and associated signaling molecules. *J*
1204 *Cell Biol* 152:959-970.
1205
- 1206 Villasana LE, Klann E, Tejada-Simon MV (2006) Rapid isolation of synaptoneurosome and
1207 postsynaptic densities from adult mouse hippocampus. *J Neurosci Methods* 158:30-36.
1208
- 1209 Wang Q, Walsh DM, Rowan MJ, Selkoe DJ, Anwyl R (2004) Block of long-term potentiation by
1210 naturally secreted and synthetic amyloid beta-peptide in hippocampal slices is mediated
1211 via activation of the kinases c-Jun N-terminal kinase, cyclin-dependent kinase 5, and
1212 p38 mitogen-activated protein kinase as well as metabotropic glutamate receptor type 5.
1213 *J Neurosci* 24:3370-3378.
1214
- 1215 Weiss LA et al. (2008) Association between microdeletion and microduplication at 16p11.2 and
1216 autism. *New Engl J Med* 358:667-675.
1217
- 1218 Whitmarsh AJ, Cavanagh L, Tournier C, Yasuda L, Davis RJ (1998) Mammalian scaffold
1219 complex that selectively mediates MAP kinase activation. *Science* 281:1671-1674.
1220
- 1221 Whitmarsh AJ, Kuan CY, Kennedy NJ, Kelkar N, Haydar TF, Mordes JP, Appel M, Rossini AA,
1222 Jones SN, Flavell RA, Rakic P, Davis RJ (2001) Requirement of the JIP1 scaffold
1223 protein for stress-induced JNK activation. *Genes Dev* 15:2421-2432.
1224
- 1225 Winchester CL, Ohzeki H, Vouyiouklis DA, Thompson R, Penninger JM, Yamagami K, Norrie
1226 JD, Hunter R, Pratt JA, Morris BJ (2012) Converging evidence that sequence variations
1227 in the novel candidate gene MAP2K7 (MKK7) are functionally associated with
1228 schizophrenia. *Human Mol Genet* 21:4910-4921.
1229
- 1230 Xia Z, Dudek H, Miranti CK, Greenberg ME (1996) Calcium influx via the NMDA receptor
1231 induces immediate early gene transcription by a MAP kinase/ERK-dependent
1232 mechanism. *J Neurosci* 16:5425-5436.
1233
- 1234 Yang DD, Kuan CY, Whitmarsh AJ, Rincon M, Zheng TS, Davis RJ, Rakic P, Flavell RA (1997)
1235 Absence of excitotoxicity-induced apoptosis in the hippocampus of mice lacking the Jnk3
1236 gene. *Nature* 389:865-870.
1237
- 1238 Yang HH, Courtney MJ, Martinsson P, Manahan-Vaughan D (2011) Hippocampal long-term
1239 depression is enhanced, depotentiation is inhibited and long-term potentiation is
1240 unaffected by the application of a selective c-Jun N-terminal kinase inhibitor to freely
1241 behaving rats. *Eur J Neurosci* 33:1647-1655.
1242
- 1243 Yang K, Trepanier C, Sidhu B, Xie YF, Li HB, Lei G, Salter MW, Orser BA, Nakazawa T,
1244 Yamamoto T, Jackson MF, MacDonald JF (2012) Metaplasticity gated through
1245 differential regulation of GluN2A versus GluN2B receptors by Src family kinases. *EMBO*
1246 *J* 31:805-816.
1247

- 1248 Yashiro K, Philpot BD (2008) Regulation of NMDA receptor subunit expression and its
1249 implications for LTD, LTP, and metaplasticity. *Neuropharmacol* 55:1081-1094.
1250
- 1251 Yin X, Feng X, Takei Y, Hirokawa N (2012) Regulation of NMDA receptor transport: a KIF17-
1252 cargo binding/releasing underlies synaptic plasticity and memory in vivo. *J. Neurosci*
1253 32:5486-5499.
1254
- 1255 Yin XL, Takei Y, Kido MA, Hirokawa N (2011) Molecular Motor KIF17 Is Fundamental for
1256 Memory and Learning via Differential Support of Synaptic NR2A/2B Levels. *Neuron*
1257 70:310-325.
1258
- 1259 Zhu Y, Pak D, Qin Y, McCormack SG, Kim MJ, Baumgart JP, Velamoor V, Auberson YP, Osten
1260 P, van Aelst L, Sheng M, Zhu JJ (2005) Rap2-JNK removes synaptic AMPA receptors
1261 during depotentiation. *Neuron* 46:905-916.
1262
- 1263 Zucker RS, Regehr WG (2002) Short-term synaptic plasticity. *Annu Rev Physiol* 64:355-405.
1264
1265

1266 **Legends**

1267

1268 **Figure 1. Analysis of JIP1 expression in the hippocampus.**

1269 (A) Fluorescent immunohistochemistry of the CA1, CA3, and DG regions of the hippocampus indicates
 1270 that JIP1 (green) predominantly co-localizes with MAP2 (red) in wild-type brain sections (*upper panels*),
 1271 suggesting relative enrichment of the JIP1 protein in neuronal processes. Co-localization between JIP1
 1272 (green) and neuron-specific nuclear protein (NeuN) (red) is sparse in the hippocampal subfields (*lower*
 1273 *panels*). Abbreviations: CA1, Cornu Ammonis 1; CA3, Cornu Ammonis 3; DG, dentate gyrus; grDG,
 1274 granular layer of DG; poDG, polymorphic layer of DG; s.l., stratum lucidum; s.l.m., stratum lacunosum
 1275 moleculare; s.p., stratum pyramidale; s.r., stratum radiatum. Scale bar = 50 μ m.

1276 (B) Nissl stain and (NeuN) stain of JIP1^{WT} and JIP1^{TA} coronal hippocampal sections. Scale bar = 200 μ m.

1277 (C,D) Pyramidal cells of the CA1 region of JIP1^{WT} and JIP1^{TA} were stained with Nissl, NeuN, the dendritic
 1278 marker MAP2, the astrocytic marker GFAP, and the inhibitory GABAergic marker GAD67 (C). The
 1279 staining was quantitated (D) (mean \pm SEM; n=4; p>0.05; Student's t-test). Scale bar = 50 μ m.

1280

1281

1282

1283 **Figure 2. Neuronal spine density and dendritic arborization of CA1 pyramidal neurons are similar**
 1284 **in JIP1^{WT} and JIP1^{TA} mice.**

1285 (A) Representative images of apical and basal dendrites spine morphology in JIP1^{TA} mice and JIP1^{WT}
 1286 littermates. Scale bar = 10 μ m.

1287 (B) Quantitation of basal and apical dendritic spine density (mean \pm SEM; n= 5 slices from 5 mice per
 1288 genotype; p>0.05, Student's t-test).

1289 (C) Quantitation of different spine types in basal and apical dendrites (mean \pm SEM, n= 5 slices from 5
 1290 mice per genotype; p>0.05, Student's t-test).

1291 (D,E) Sholl analysis of dendritic arborization of CA1 pyramidal neurons. Values on the x-axis represent
 1292 increasing distance from the soma of the pyramidal cells. Basal and apical dendrites of pyramidal cells
 1293 from n= 5 slices from 5 mice per genotype were examined (mean \pm SEM; p>0.05, Student's t-test).

1294

1295

1296

1297 **Figure 3. JIP1-dependent JNK activation in the hippocampus is suppressed in JIP1^{TA} mice.**

1298 (A-C) JIP1^{WT} and JIP1^{TA} mice were treated by systemic injection of kainate. At 2 h post-treatment,
 1299 sections of the brain were prepared and stained (green) with antibodies to pSer⁶³ cJun (A), cJun (B), or
 1300 cFos (C). DNA was stained with DAPI (red). Representative sections of the dentate gyrus of the
 1301 hippocampus are presented. Scale bar = 75 μ m.

1302 (D,E) Extracts prepared from the hippocampus of JIP1^{WT} and JIP1^{TA} mice treated with kainate (0 – 60
 1303 mins) were examined by multiplexed ELISA to measure the amount of pSer⁶³-cJun (D) and cJun (E)
 1304 normalized to the amount of JNK. The data presented are the mean \pm SEM (n=5; **, p<0.01, two-way
 1305 ANOVA followed by Bonferroni's post-hoc test).

1306

1307

1308

1309 **Figure 4. JIP1^{TA} mice exhibit reduced JNK activation in the dorsal hippocampus following**
 1310 **contextual fear conditioning.**

1311 Dorsal hippocampal tissue was isolated from naïve mice and from mice at different times after contextual
 1312 fear conditioning (FC) and examined by immunoblot analysis by probing with antibodies to phospho-JNK,
 1313 JNK, and GAPDH. The amount of 46-kDa and 54-kDa phospho-JNK was quantitated and normalized to
 1314 the amount of JNK in each sample (mean \pm SEM; n=5; ***, p<0.001, for JIP1^{TA} compared with JIP1^{WT}
 1315 mice; #, p<0.01, ##, p<0.001 compared with the naïve control, two-way ANOVA, followed by Bonferroni's
 1316 post-hoc test

1317

1318

1319

1320 **Figure 5. The threshold for LTP induction is reduced in JIP1^{TA} mice.**

1321 **(A,B)** Basal synaptic transmission at Schaffer collateral-CA1 synapses, as assessed by measuring the
 1322 fEPSP input-output relationship (A) and the fEPSP slope to fiber volley relationship (B), was similar in
 1323 JIP1^{TA} slices (n = 16 slices, 13 mice) compared with slices obtained from JIP1^{WT} littermates (n = 16
 1324 slices, 12 mice). No statistically significant differences were found (p>0.05, two-way repeated measures
 1325 ANOVA).

1326 **(C)** fEPSPs from JIP1^{TA} (n = 16 slices, 13 mice) and JIP1^{WT} (n = 16 slices, 12 mice) slices exhibited
 1327 similar paired pulse facilitation. No statistically significant differences were found (p>0.05, two-way
 1328 repeated measures ANOVA).

1329 **(D)** High-frequency stimulation LTP was induced by two trains of 100 Hz stimulation (separated by a 20
 1330 sec interval) to the Schaffer collaterals in slices from JIP1^{TA} and JIP1^{WT} mice (n = 10 slices, 8
 1331 mice/genotype). Stimulation was delivered at time 0 (arrow). No statistically significant differences were
 1332 found (p>0.05, Student's t-test).

1333 **(E)** An intermediate-stimulation LTP protocol involved 900 pulses of 10 Hz stimuli delivered at time 0.
 1334 LTP induced at intermediate frequencies was significantly facilitated in slices taken from JIP1^{TA} mice
 1335 when compared to JIP1^{WT} controls (n = 10 slices, 9 mice/genotype). Statistically significant differences are
 1336 indicated (***, p<0.001, Student's t-test).

1337 **(F)** LTD induced by low-frequency (1 Hz, 900 pulses, 0-15 min time) stimulation was significantly reduced
 1338 in JIP1^{TA} slices compared to JIP1^{WT} slices (n = 10 slices, 10 mice/genotype). Statistically significant
 1339 differences are indicated (***, p<0.0001, Student's t-test).

1340 **(G)** LTD induced by 0.5 Hz stimulation (0.5 Hz, 900 pulses, 0-30 min time) was similar in JIP1^{WT} and
 1341 JIP1^{TA} slices (n = 14 slices, 11 mice/genotype). No statistically significant differences were found
 1342 (p>0.05, Student's t-test).

1343 **(H)** Frequency-response function in JIP1^{TA} and JIP1^{WT} mice. The percentage change in synaptic
 1344 strength from baseline in JIP1^{TA} and JIP1^{WT} mice at 50-60 min following stimulation at the indicated
 1345 frequency is presented. Values are mean \pm SEM. Magnitudes of LTP/LTD were calculated as the ratio of
 1346 the average fEPSPs between 50-60 min and average baseline fEPSPs between -20 min -0 min.
 1347 Statistically significant differences are indicated (***, p<0.001, Student's t-test).

1348 **(I)** mGluR-dependent LTP in hippocampal slices from JIP1^{TA} and JIP1^{WT} mice. mGluR-LTD was induced
 1349 by incubation of JIP1^{TA} and JIP1^{WT} slices with DHPG (100 μ M) for 5 min (n = 10 slices, 10 mice/genotype).
 1350 Basal fEPSPs were recorded prior to LTD induction with DHPG. No statistically significant differences
 1351 were found (p>0.05, Student's t-test).

1352 **(J)** Depotentiation is not affected in JIP1^{TA} mice. High-frequency stimulation (100 Hz twice for 1 s with 20
 1353 s interval), followed with 1 Hz (15 min) stimulation 10 min later to the Schaffer collaterals produced similar
 1354 depotentiation in slices from JIP1^{TA} and JIP1^{WT} mice (n = 10 slices, 10 mice/genotype). No statistically
 1355 significant differences were found (p>0.05, Student's t-test).

1356 The insets in D-J show representative fEPSP responses obtained before and after LTP, LTD and
 1357 depotentiation inducing stimuli. (Calibration: 0.2 mV/10 ms).

1358

1359

1360

1361 **Figure 6. Inhibition of JNK signaling mimics the effect of JIP1 (Thr¹⁰³Ala) mutation on NMDA**
 1362 **receptor-dependent LTD.**

1363 **(A, B)** JNK-in-8 treatment did not affect baseline synaptic transmission or paired-pulse facilitation in wild-
 1364 type slices. Input–output curves, as assessed by the fEPSP slope to fiber volley relationship, were similar
 1365 in vehicle-treated slices (n = 12 slices) compared with wild-type slices treated with JNK-in-8 (n = 12
 1366 slices) (A). fEPSPs from vehicle-treated slices (n = 12 slices) and JNK-in-8 treated (n = 12 slices) slices
 1367 exhibited similar paired pulse facilitation (PPF) (B) (p>0.05, two-way repeated measures ANOVA).

1368 **(C)** High-frequency stimulation (HFS)-LTP was induced with a pair of 100 Hz tetani in the presence of
 1369 either vehicle (n = 12) or 6 μM JNK-in-8 (n = 12). LTP was unaffected by JNK inhibition. (p> 0.05,
 1370 Student's t-test).

1371 **(D)** Low-frequency stimulation (LFS)-LTD was induced (1 Hz, 900 pulses) in the presence of either
 1372 vehicle (n = 10) or 6 μM JNK-in-8 (n = 10). LTD was impaired by JNK inhibition (***, p<0.001, Student's
 1373 t-test).

1374 The insets in C and D show representative fEPSP responses obtained before and after LTP/LTD inducing
 1375 stimuli. (Calibration: 0.2 mV/10 ms).

1376

1377

1378

1379 **Figure 7. The JIP1^{TA} mutation promotes increased NMDA receptor expression and activity.**

1380 **(A-C)** Lysates prepared from the hippocampi of JIP1^{TA} and JIP1^{WT} mice were examined by immunoblot
 1381 analysis by probing with antibodies to NMDA and AMPA receptor subunits, SAP102, JIP1, and β-tubulin
 1382 (A). The amount of NMDA receptor subunits in the hippocampus was quantitated and normalized to the
 1383 amount of β-tubulin in each sample (B, mean ± SEM, n = 5; **, p<0.01, Student's t-test). The amount of
 1384 NMDA receptor subunit mRNA in the hippocampus was measured by quantitative RT-PCR and
 1385 normalized to the amount of *Gapdh* mRNA in each sample (C, mean ± SEM, n = 5; p>0.05, Student's t-
 1386 test).

1387 **(D)** Enrichment of NMDA receptor subunits in the synaptoneurosome fraction of the hippocampus of
 1388 JIP1^{WT} and JIP1^{TA} mice was examined by immunoblot analysis.

1389 **(E,F)** Primary JIP1^{WT} and JIP1^{TA} hippocampal neurons were fixed and processed for
 1390 immunofluorescence analysis under non-permeabilized (*left panels*) and permeabilized (*right panels*)
 1391 conditions. GluN1 surface and intracellular expression was examined by confocal microscopy (E).
 1392 Quantitation of the cell surface expression of GluN1 in JIP1^{TA} and JIP1^{WT} hippocampal neurons was
 1393 performed using ImageJ software (F). The data presented are the mean ± SEM; n = 8–10; **, p<0.01,
 1394 Student's t-test).

1395 **(G)** The expression of *cJun* and *cFos* mRNA in the hippocampus of JIP1^{WT} and JIP1^{TA} mice was
 1396 normalized to the amount of *Gapdh* in each sample (mean ± SEM, n = 5–6). Statistically significant
 1397 differences are indicated (**, p<0.01, Student's t test).

1398 **(H)** Lysates prepared from the hippocampus of JIP1^{WT} and JIP1^{TA} mice were examined by immunoblot
 1399 analysis with antibodies to phospho-ERK, ERK, phospho-CREB, CREB, KIF17, and β-Tubulin. The
 1400 amount of phospho-ERK and phospho-CREB was quantitated (mean ± SEM, n = 5). Statistically
 1401 significant differences are indicated (**, p<0.01, Student's t-test).

1402 **Figure 8. Increased synaptic NMDA receptor activity in hippocampal slices from JIP1^{TA} mice.**

1403 **(A)** Whole-cell voltage clamp traces depicting typical EPSCs elicited by stimulating the Schaffer
 1404 collaterals while recording CA1 pyramidal cells from JIP1^{WT} and JIP1^{TA} hippocampal slices. Strong
 1405 blockade of NMDA receptors at a holding potential of -70 mV by magnesium isolates the AMPA

1406 component (*lower traces*). The +50 mV upper traces primarily represent the NMDA component because
 1407 the traces were recorded 30-50 msec after stimulation when approximately 90% of the AMPA receptor
 1408 response had decayed. The traces show the increase in the NMDA receptor-mediated component for the
 1409 JIP1^{TA} group relative to JIP1^{WT}, while AMPA receptor mediated responses were not different. Traces
 1410 depicted are averages of 20 sweeps for both NMDA and AMPA receptor-mediated components of JIP1^{WT}
 1411 recorded from the same pyramidal neuron; 10 and 15 sweeps were used to produce the averages
 1412 depicted for the NMDA and AMPA receptor-mediated components recorded from a JIP1^{TA} pyramidal
 1413 neuron.

1414 (B,C) Comparison of average NMDA and AMPA receptor currents. NMDA receptor-mediated currents
 1415 (B) were significantly greater in the JIP1^{TA} group in comparison to the JIP1^{WT} group (mean ± SEM; n = 16
 1416 ~ 17 cells; *, p<0.05, Student's t-test) while average AMPA receptor-mediated currents (C) did not differ.

1417 (D) NMDA to AMPA receptor current ratios were evaluated on a cell-by-cell basis. The JIP1^{TA} ratios
 1418 ($I_{\text{NMDA}} / I_{\text{AMPA}}$) were larger than ratios measured from neurons in the JIP1^{WT} group (mean ± SEM; n = 16 ~
 1419 17 cells; *, p<0.05, Student's t-test).

1420 (E,F) NMDA-stimulated gene expression in primary cultures of JIP1^{WT} and JIP1^{TA} hippocampal neurons
 1421 was studied by treating neurons with 100 μM NMDA plus 10 μM glycine. The expression of *Bdnf* (E) and
 1422 *cFos* (F) mRNA was quantitated by RT-PCR and normalized to *Gapdh* (mean ± SEM; n= 5-6; ***,
 1423 p<0.001, two-way ANOVA followed by Bonferroni's post-hoc test).

1424

1425

1426

1427 **Figure 9. JIP1^{TA} mice display normal locomotor function, motor coordination, elevated anxiety-like**
 1428 **behavior and increased acoustic startle response.**

1429 (A-C) Elevated Plus Maze. JIP1^{TA} mice show decreased time spent in open arms (A), increased time
 1430 spent in closed arms (B) relative to wild-type mice, indicative of elevated anxiety-like behaviors. In
 1431 addition, JIP1^{TA} mice show normal activity as measured by total distance traveled (C). The data are
 1432 presented as the mean ± SEM (n = 10; **, p<0.01, Student's t-test).

1433 (D,E) Open Field Test. JIP1^{TA} mice show increased anxiety-like behavior in an open field test. Mice
 1434 were allowed to explore an open field for 5 min. JIP1^{TA} mice spent more time in the periphery (D) and less
 1435 time in the center region of the open field (E), both indicators of increased levels of anxiety-like behavior
 1436 in this test. The data are presented as the mean ± SEM (n = 10; ***, p<0.001, Student's t-test).

1437 (F) JIP1^{TA} mice showed an increased acoustic startle response for the 110 dB acoustic startle stimulus
 1438 compared with JIP1^{WT} mice (mean ± SEM; n = 8; *, p<0.05, two-way repeated measures ANOVA
 1439 followed by Bonferroni's post-hoc comparisons tests).

1440 (G) No significant differences in prepulse inhibition for the 74, 80 and 86 dB pre-pulse sound levels
 1441 followed by a 110 dB startle stimulus were observed between JIP1^{TA} and JIP1^{WT} mice (mean ± SEM; n =
 1442 8; p>0.05, two-way repeated measures ANOVA followed by Bonferroni's post-hoc test).

1443 (H) JIP1^{TA} mice have normal balance and motor coordination, but impaired skill learning on the rotarod.
 1444 Mice received four trials on day 1 (Trials 1-4) and day 2 (Trials 5-8). The duration of balance or latency to
 1445 fall (4-40 rpm over 5 min) was recorded. Mice were trained on day 1 to establish baseline performance,
 1446 and retested 24 hours later to measure skill learning. Both JIP1^{TA} and JIP1^{WT} mice exhibited increased
 1447 skill in maintaining balance on the rotarod over the first four trials on day 1. On day 2, JIP1^{TA} mice failed
 1448 to display motor coordination achieved after the day 1, indicative of impaired motor learning in the rotarod
 1449 task. Data are presented as mean ± SEM; n = 8; *, p<0.05, two-way repeated measures ANOVA
 1450 followed by Bonferroni's post-hoc test.

1451

1452

1453

1454 **Figure 10. JIP1^{TA} mice display enhanced contextual fear and impaired fear extinction.**

1455 (A) “Strong” (0.8 mA electric shock) training demonstrated that JIP1^{TA} and JIP1^{WT} littermate mice
 1456 exhibited similar contextual freezing when tested immediately after training, or 1 h later, but the JIP1^{TA}
 1457 mice froze more than JIP1^{WT} mice at 24 h following training (left panel). Foot-shock reactivity during fear
 1458 conditioning training did not significantly differ between JIP1^{TA} and JIP1^{WT} mice (right panel). The data
 1459 presented are the mean ± SEM (n = 10 ~ 11; ***, p<0.001, Student’s t-test).

1460 (B) “Weak” (0.4 mA electric shock) training demonstrated that JIP1^{TA} mice (n = 14) exhibited contextual
 1461 freezing that was similar to the “strong” training schedule, but JIP1^{WT} mice (n = 14) displayed significantly
 1462 less contextual fear conditioning at 24 h following training (mean ± SEM; n = 14; ***, p<0.001, Student’s t-
 1463 test).

1464 (C) JIP1^{TA} and JIP1^{WT} littermate mice were infused with vehicle or the selective NMDA receptor
 1465 antagonist APV (10 µg/ml) before “strong” (0.8 mA) contextual fear conditioning. The following day, there
 1466 was a similar impairment in both genotypes in freezing levels to the conditioning context (mean ± SEM; n
 1467 = 10; ***, p<0.001 vs. JIP1^{WT+veh.}; not significant (ns) JIP1^{WT+APV} vs. JIP1^{TA+APV}; two-way ANOVA followed
 1468 by Bonferroni’s post-hoc test).

1469 (D) JIP1^{TA} and JIP1^{WT} littermate mice were trained by “strong” (0.8 mA electric shock) contextual fear
 1470 conditioning. Extinction began 24 h later and consisted of daily 3-min re-exposures of mice to the
 1471 conditioning context in the absence of shock. When compared with JIP1^{WT} littermates, JIP1^{TA} mice
 1472 showed increased freezing behavior throughout extinction days 1-7 (E1-E7), indicating impaired
 1473 extinction process in JIP1^{TA} mice (mean ± SEM; n = 10; *, p<0.05, ***, p<0.001; two-way repeated
 1474 measures ANOVA followed by Bonferroni’s post-hoc test).

1475 (E) “Weak” (0.4 mA electric shock; left panel) and “strong” (0.8 mA; right panel) cued fear training,
 1476 consisting of a single pair of cue (tone) and shock, demonstrated that JIP1^{TA} and JIP1^{WT} mice exhibited
 1477 enhanced conditioned freezing to a cue, tone, when tested 24 h following training (mean ± SEM; n = 11;
 1478 *, p<0.05, **, p<0.01, Student’s t-test).

1480

1481

1482

1483 **Figure 11. JIP1^{TA} mice exhibit enhanced acquisition and reversal learning in the Morris water**
 1484 **maze test.**

1485 (A-C) JIP1^{TA} and JIP1^{WT} littermate mice learned the visible platform task (day 1 & 2), as indicated by
 1486 reductions in escape time during training. The mice were then trained to find a hidden platform during the
 1487 next seven days. JIP1^{TA} mice showed faster escape latencies at days 6-9 training compared with JIP1^{WT}
 1488 littermates (A). A first probe test (day 10) was conducted 24 h after the completion of training. No
 1489 significant differences in percentage time spent in the target quadrant (T) between JIP1^{TA} and JIP1^{WT}
 1490 mice were observed (B). The mice were then subjected to 2 days of additional training (days 11-12), and
 1491 a second probe trial was performed 24 h later. No significant differences between JIP1^{TA} and JIP1^{WT}
 1492 mice were observed during second probe trial (C). Data presented are the mean ± SEM (n = 14; *,
 1493 p<0.05, two-way repeated measures ANOVA, followed by Bonferroni’s post-hoc test).

1494 (D-F) Twenty-four hours after the second probe test, the platform was moved to the opposite quadrant in
 1495 the pool and mice were trained for four trials (day 14, reversal learning). In this new setting, JIP1^{TA} mice
 1496 displayed shorter escape time to find newly placed platform (NT) compared with JIP1^{WT} littermate mice
 1497 (E). The probe test for reversal training was conducted 24 h after the completion of new platform training
 1498 (day 15). Analysis of the time spent in the quadrants revealed that JIP1^{TA} mice spent significantly more
 1499 time in the new target quadrant than JIP1^{WT} mice (F). Data presented are the mean ± SEM (n = 14; *,
 1500 p<0.05, ***, p<0.001, two-way repeated measures ANOVA (E) and two-way ANOVA (F) followed by
 1501 Bonferroni’s post-hoc tests).

1502

1503

1504

1505

1506 **Figure 12. Suppression of kainate-induced JNK activity in the hippocampus of JIP1^{ΔJBD} mice.**

1507 (A,B) A targeting vector was designed to replace JIP1 residues Leu¹⁶⁰-Asn¹⁶¹-Leu¹⁶² with Gly¹⁶⁰-Arg¹⁶¹-
 1508 Gly¹⁶² in exon 3 of the *Jip1* gene by homologous recombination in ES cells. The *floxed Neo^R* cassette
 1509 inserted in intron 3 and used for selection was deleted with *Cre* recombinase. H, HindIII.

1510 (C) Lysates prepared from the cerebral cortex of *Jip1*^{+/+} (WT) and *Jip1*^{ΔJBD/ΔJBD} (ΔJBD) mice were
 1511 examined by immunoblot analysis using antibodies to JIP1 and β-Tubulin.

1512 (D,E) JIP1^{WT} and JIP1^{ΔJBD} mice were treated without and with kainate. Representative sections of the
 1513 dentate gyrus stained (green) with antibodies to phospho-cJun (D) or cJun (E) are presented. DNA was
 1514 stained with DAPI (red). Scale bar = 75 μm.

1515

1516

1517

1518 **Figure 13. Disruption of the JNK binding domain (ΔJBD) on JIP1 causes enhanced associative**1519 **learning.**

1520 (A) Contextual and cued fear conditioning of JIP1^{ΔJBD} and JIP1^{WT} mice consisted of one exposure to cue
 1521 [context + tone] and 0.8mA shock (mean ± SEM; n = 10-11; **, p<0.01, Student's t-test ***, p<0.001,
 1522 Student's t-test).

1523 (B,C) Morris water maze tests of mean latencies to escape to a visible (days 1-2) or a hidden platform
 1524 (days 3-12) are presented for JIP1^{ΔJBD} or JIP1^{WT} mice (B). Probe trials were performed on days 9 and 13
 1525 of water maze training (C). JIP1^{ΔJBD} mice spent significantly longer time in the target quadrant compared
 1526 to JIP1^{WT} littermates (mean ± SEM; n = 10; *, p<0.05; **, p<0.01; ***, p<0.001, two-way repeated
 1527 measures ANOVA (B) and two-way ANOVA (C) followed by Bonferroni's post-hoc tests).

1528 (D) The water maze platform was moved to the opposite quadrant in the pool and mice were trained for
 1529 four trials (day 14, reversal learning). The probe test for reversal training was conducted 24 h after the
 1530 completion of new platform training (day 15). Analysis of the time spent in the quadrants during the probe
 1531 trial revealed that JIP1^{ΔJBD} mice spent significantly more time in the new target quadrant (NT) than JIP1^{WT}
 1532 mice (mean ± SEM; n = 10; ***, p<0.001, two-way ANOVA followed by Bonferroni's post-hoc test).

1533 (E) Hippocampus lysates of JIP1^{WT}, JIP1^{TA} and JIP1^{ΔJBD} mice were examined by immunoblot analysis by
 1534 probing with antibodies to NMDA receptor subunits and β-Tubulin.

1535 (F) The amount of phospho-ERK in hippocampus lysates of naïve JIP1^{WT} and JIP1^{ΔJBD} mice was
 1536 quantified by multiplexed ELISA and normalized to the amount of ERK2 in each sample (mean ± SEM; n
 1537 = 5; *, p<0.05, Student's t-test).

1538

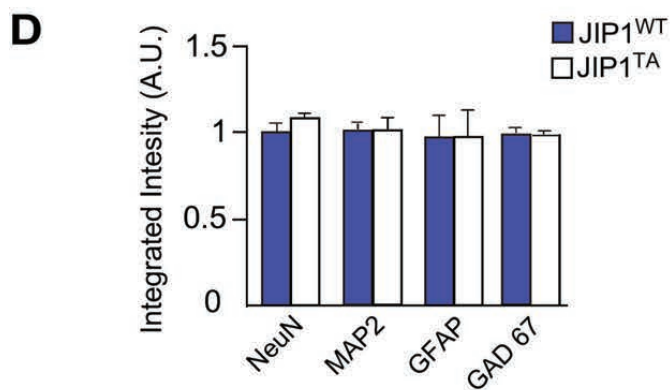
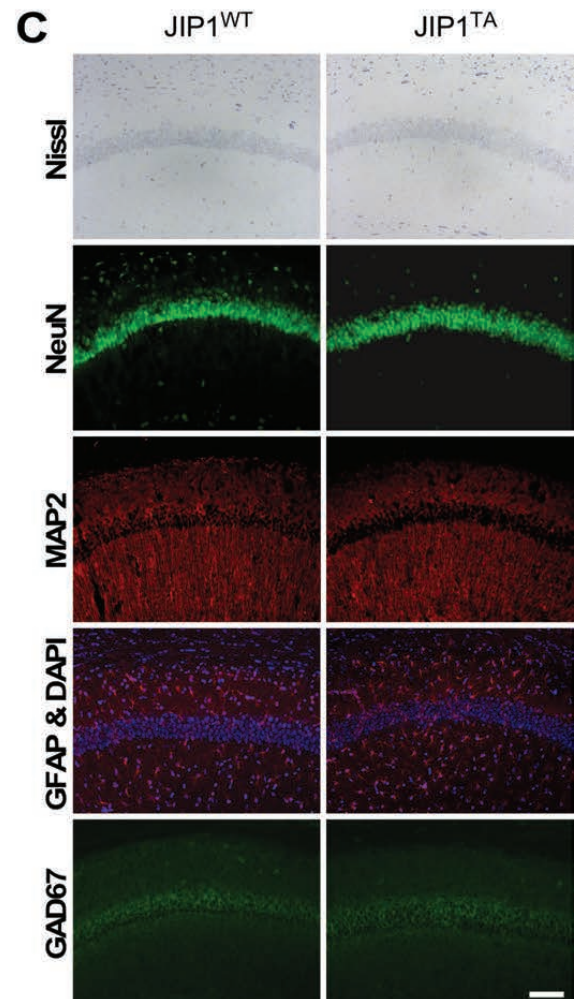
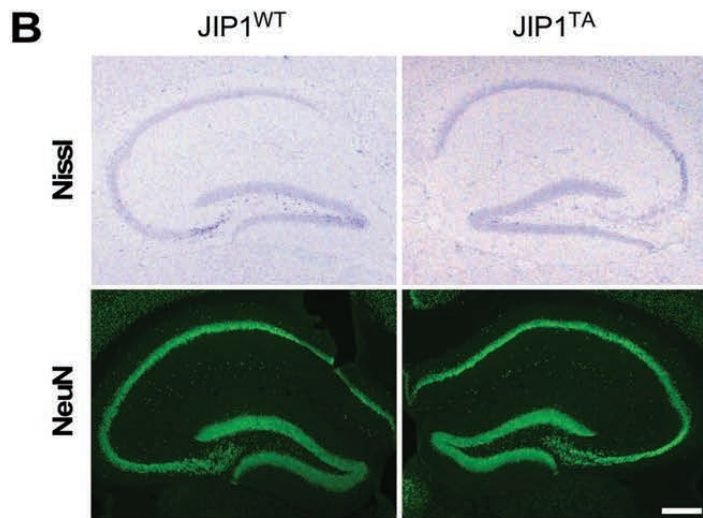
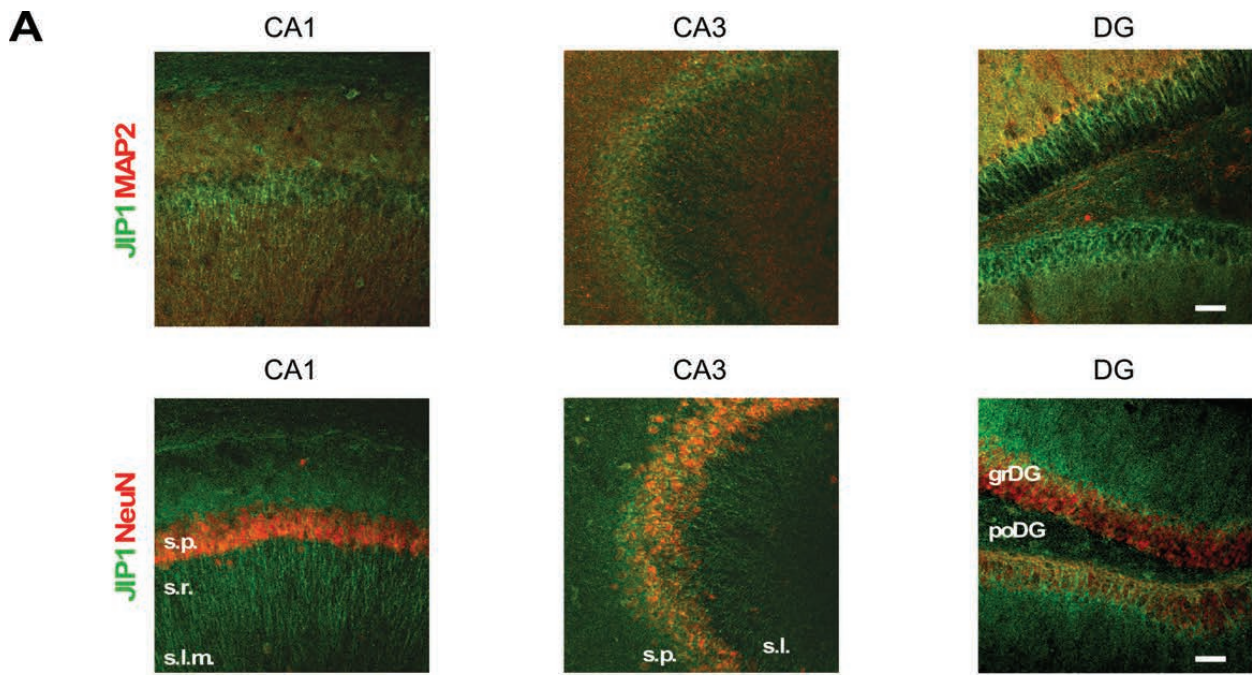
1539

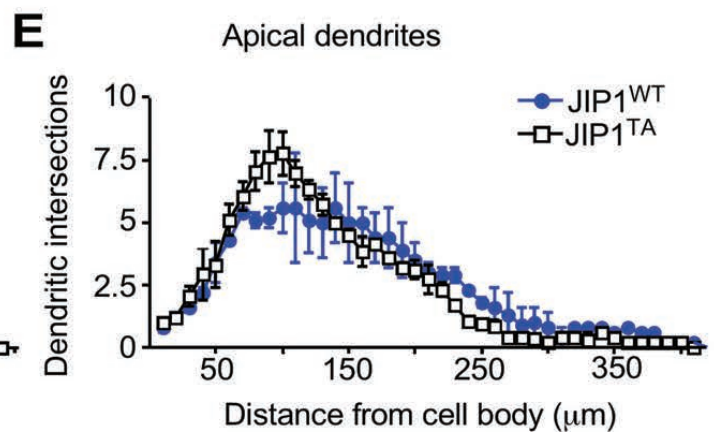
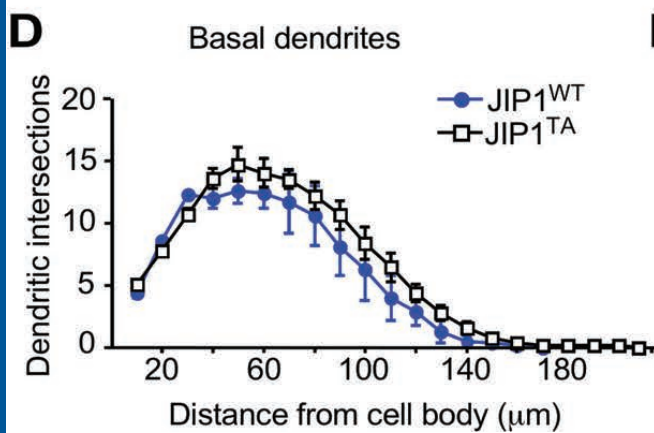
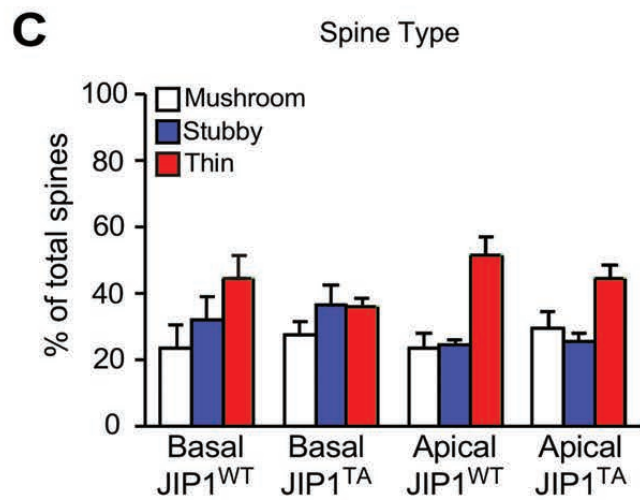
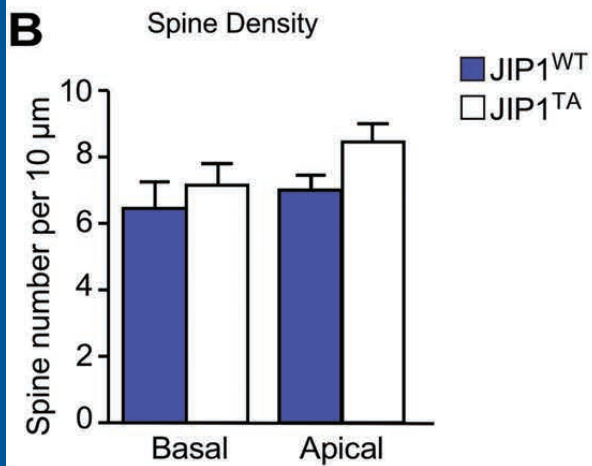
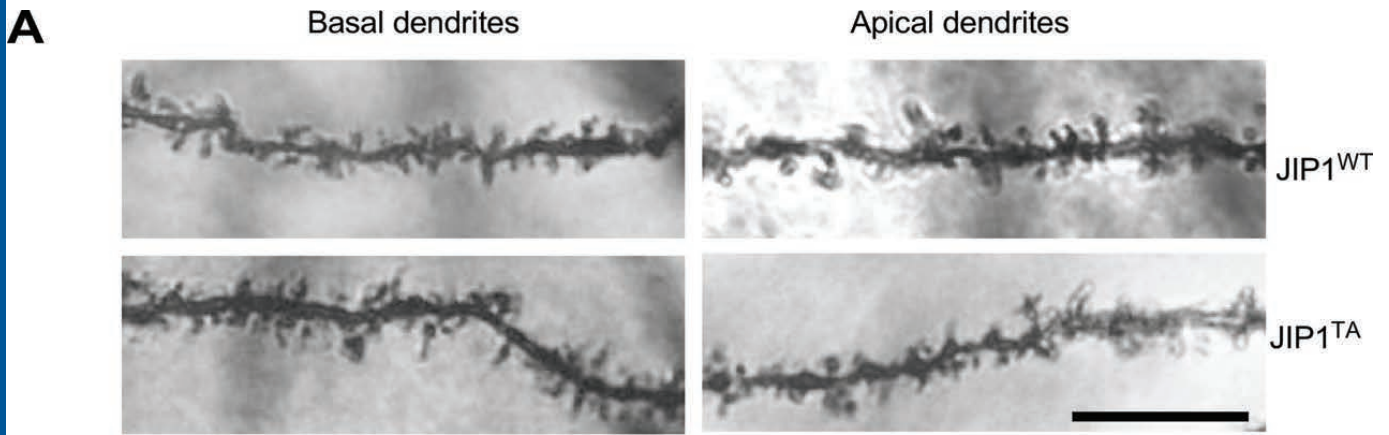
1540

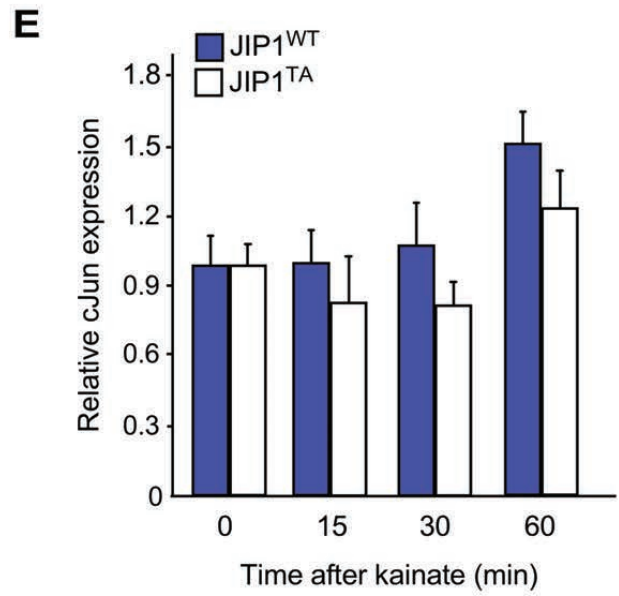
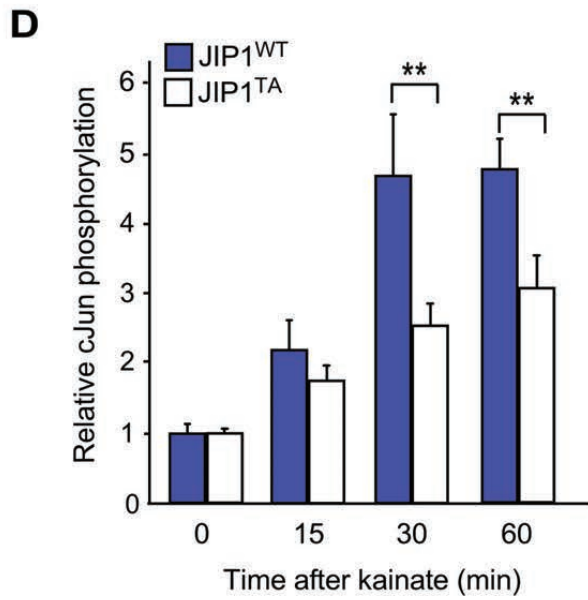
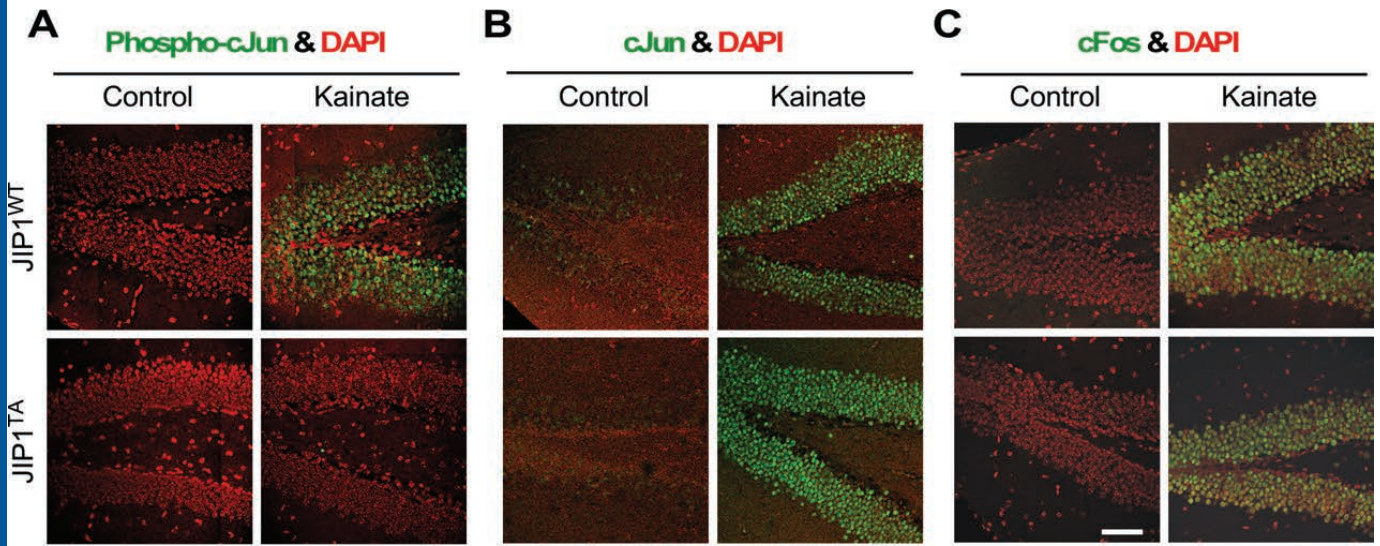
1541

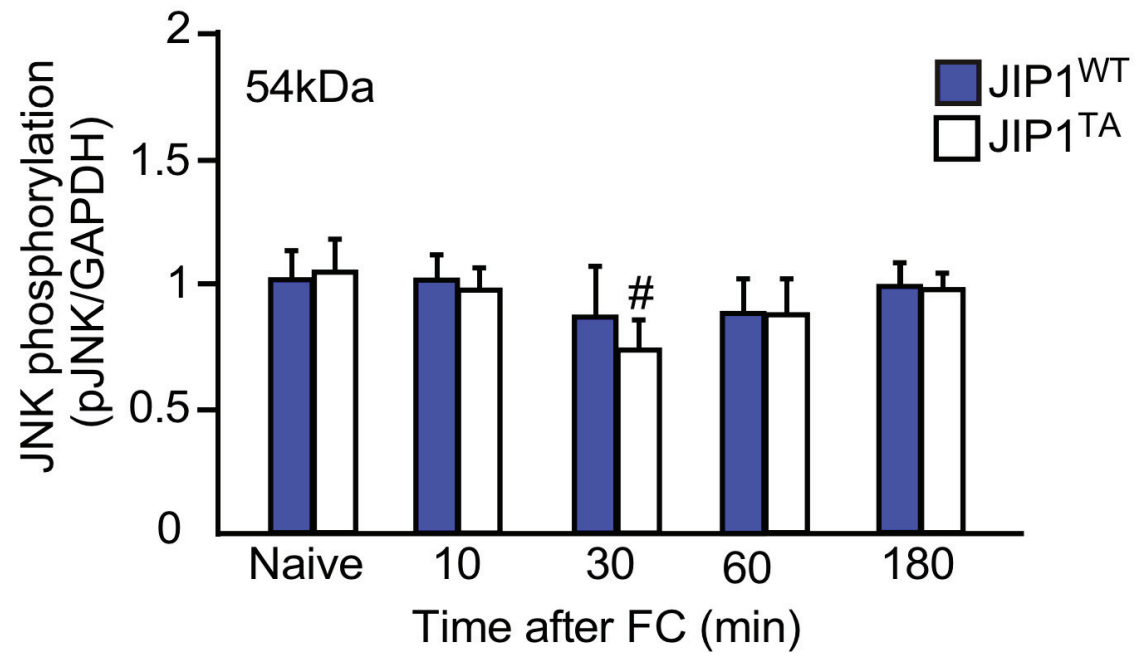
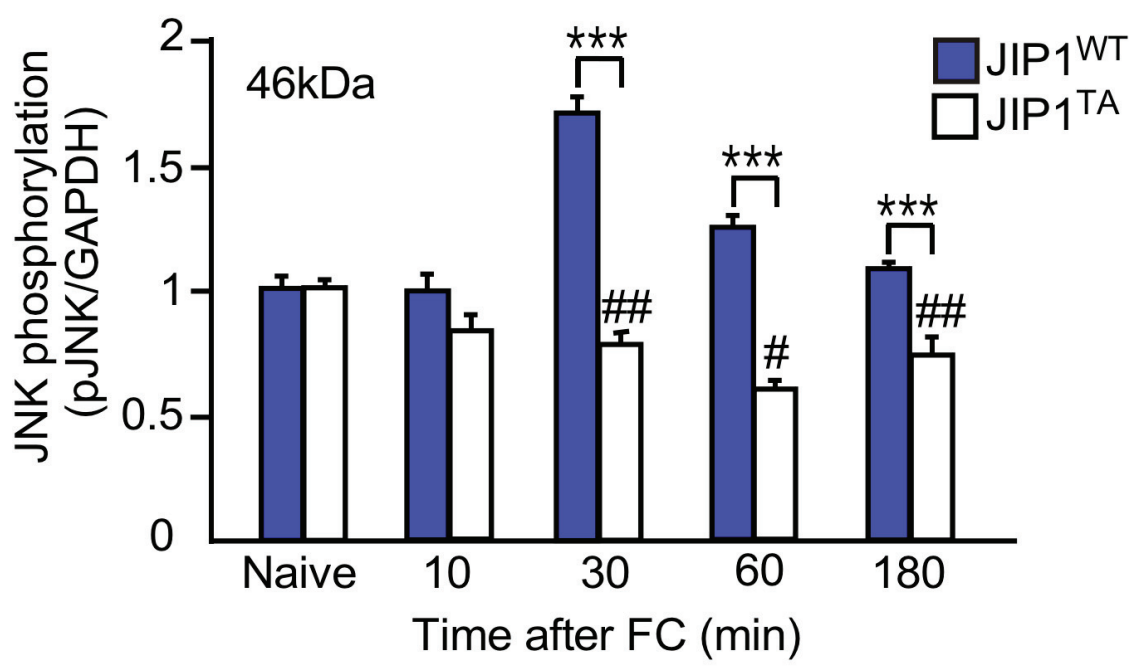
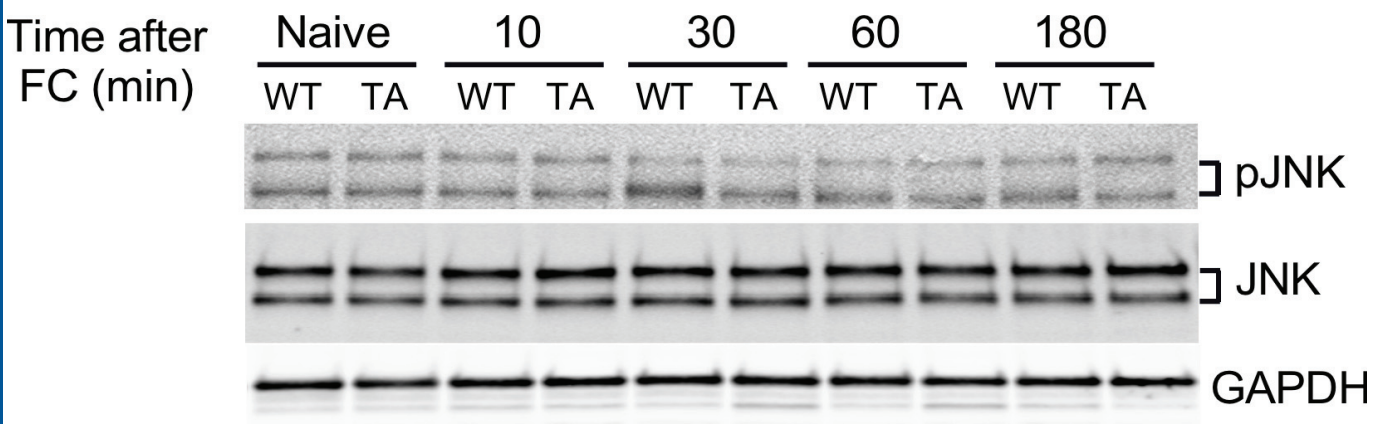
1542 **Figure 14. A model of how JIP1-mediated JNK signaling regulates synaptic NMDA receptor**

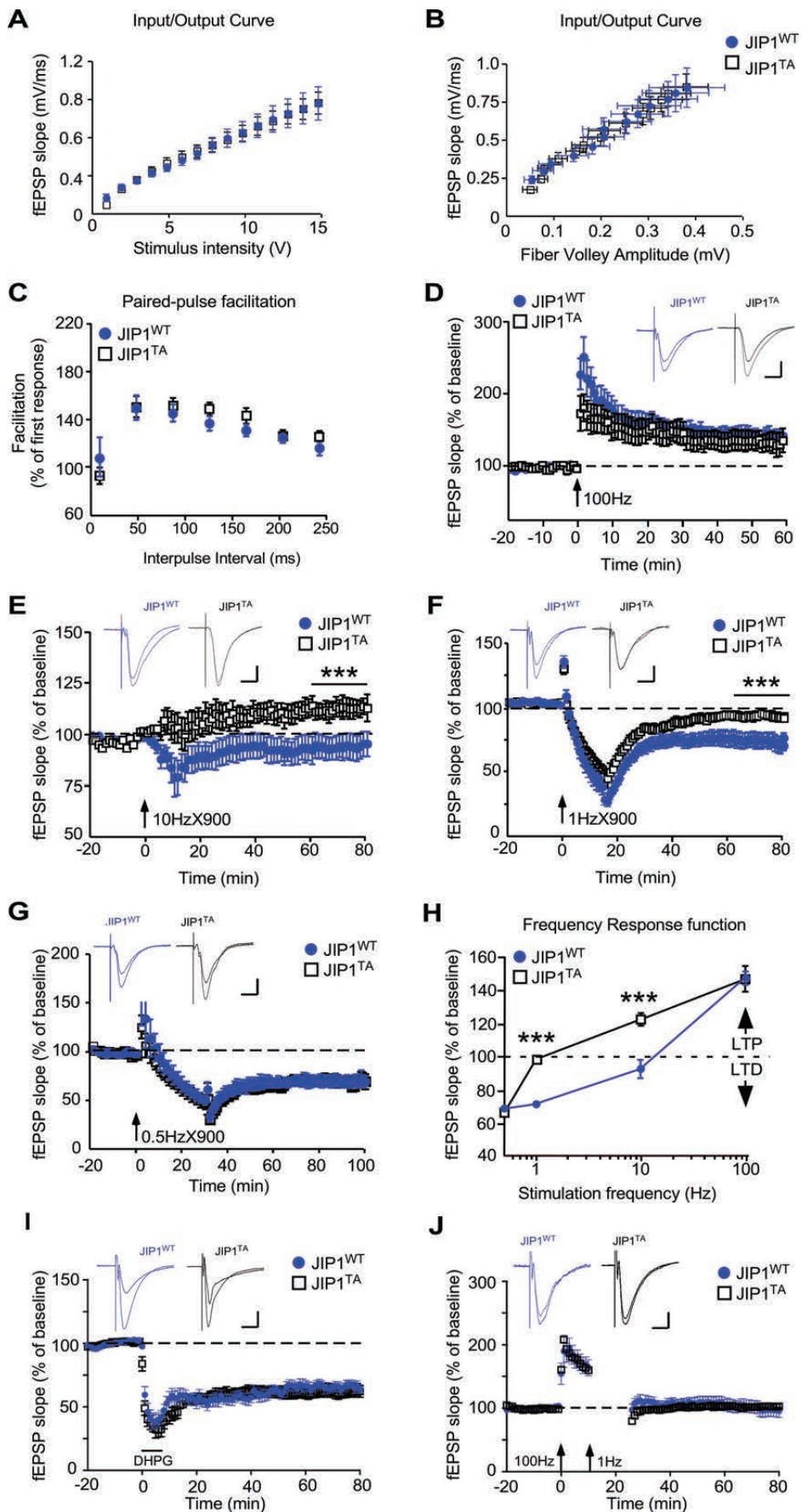
1543 **expression.** JIP1-dependent JNK activation by the NMDA receptor (NMDAR) may suppress translation
 1544 of NMDA receptor subunit mRNA (*Grin1*, *Grin2a*, *Grin2b*). Alternatively, the same pathway regulates cell
 1545 surface insertion or retrieval of NMDA receptors and/or lateral diffusion of extrasynaptic NMDA receptors
 into synaptic sites.

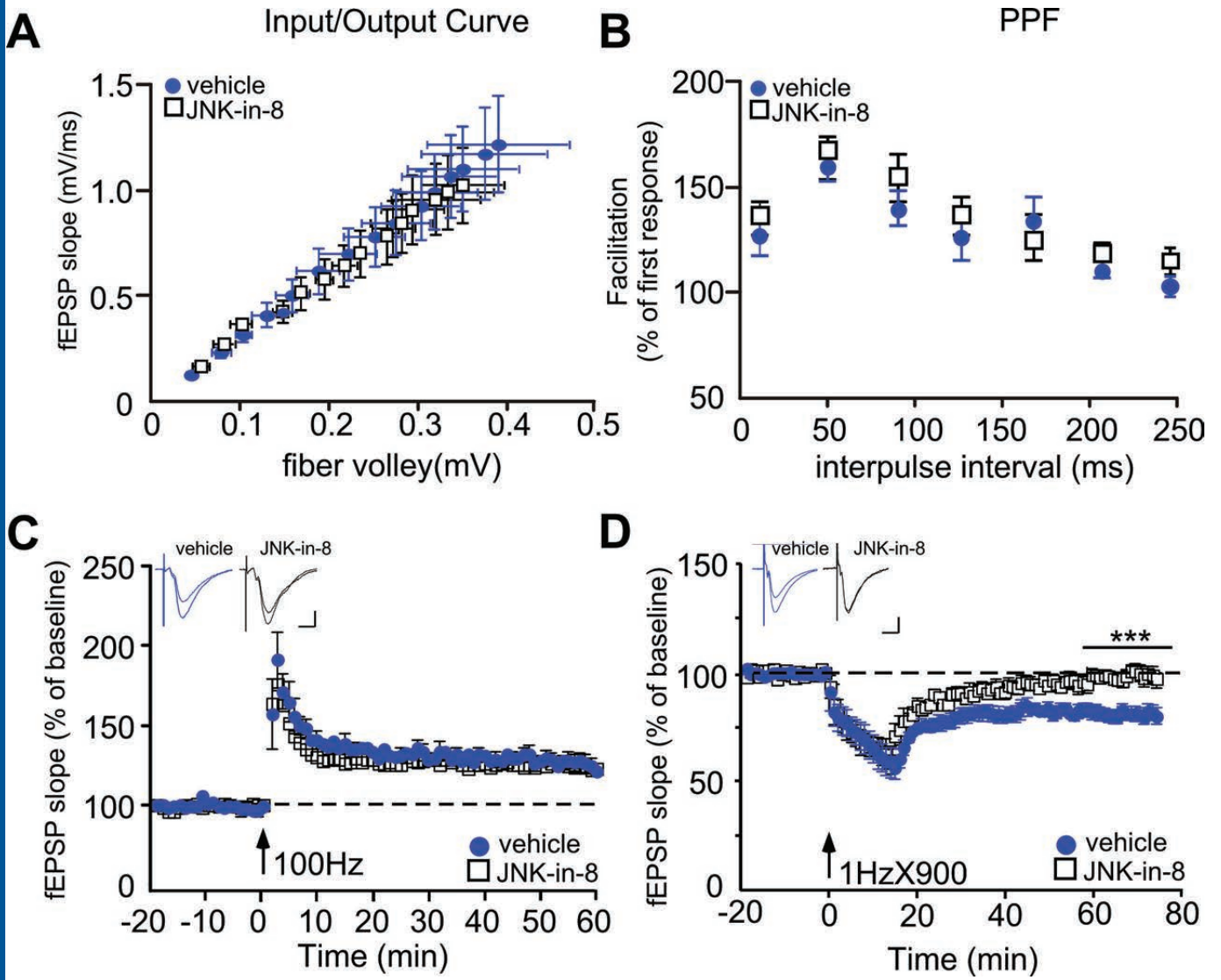


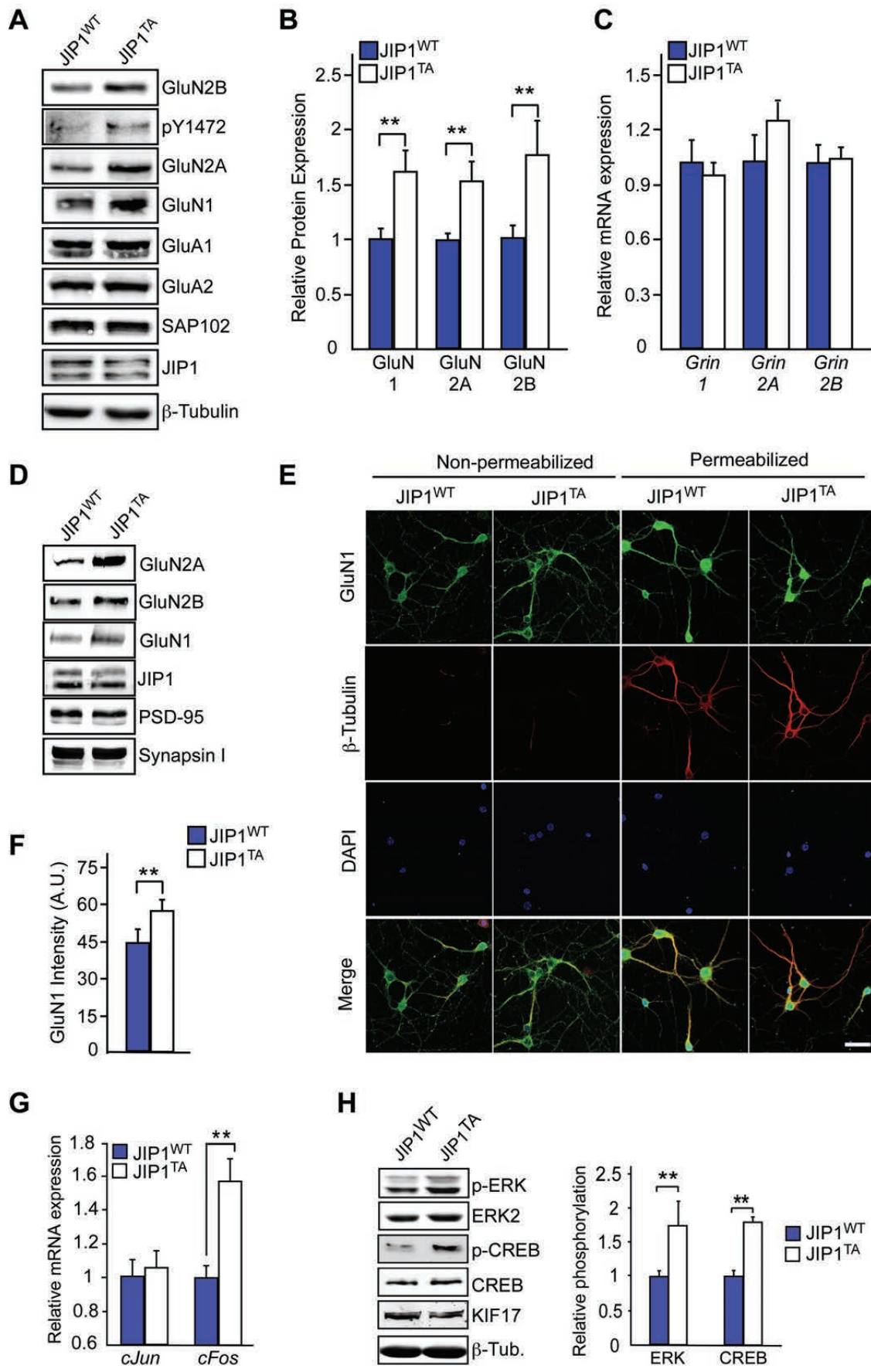


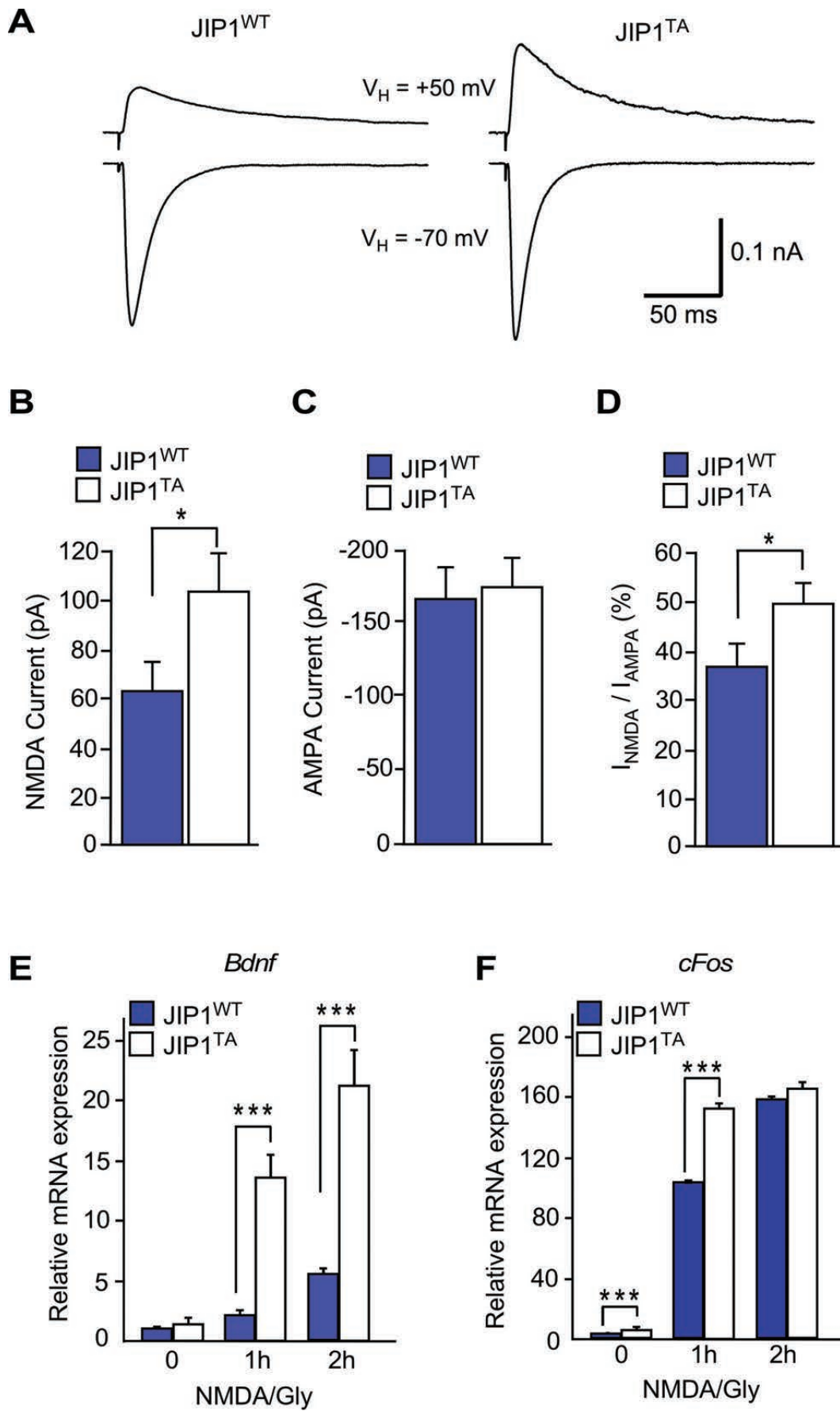


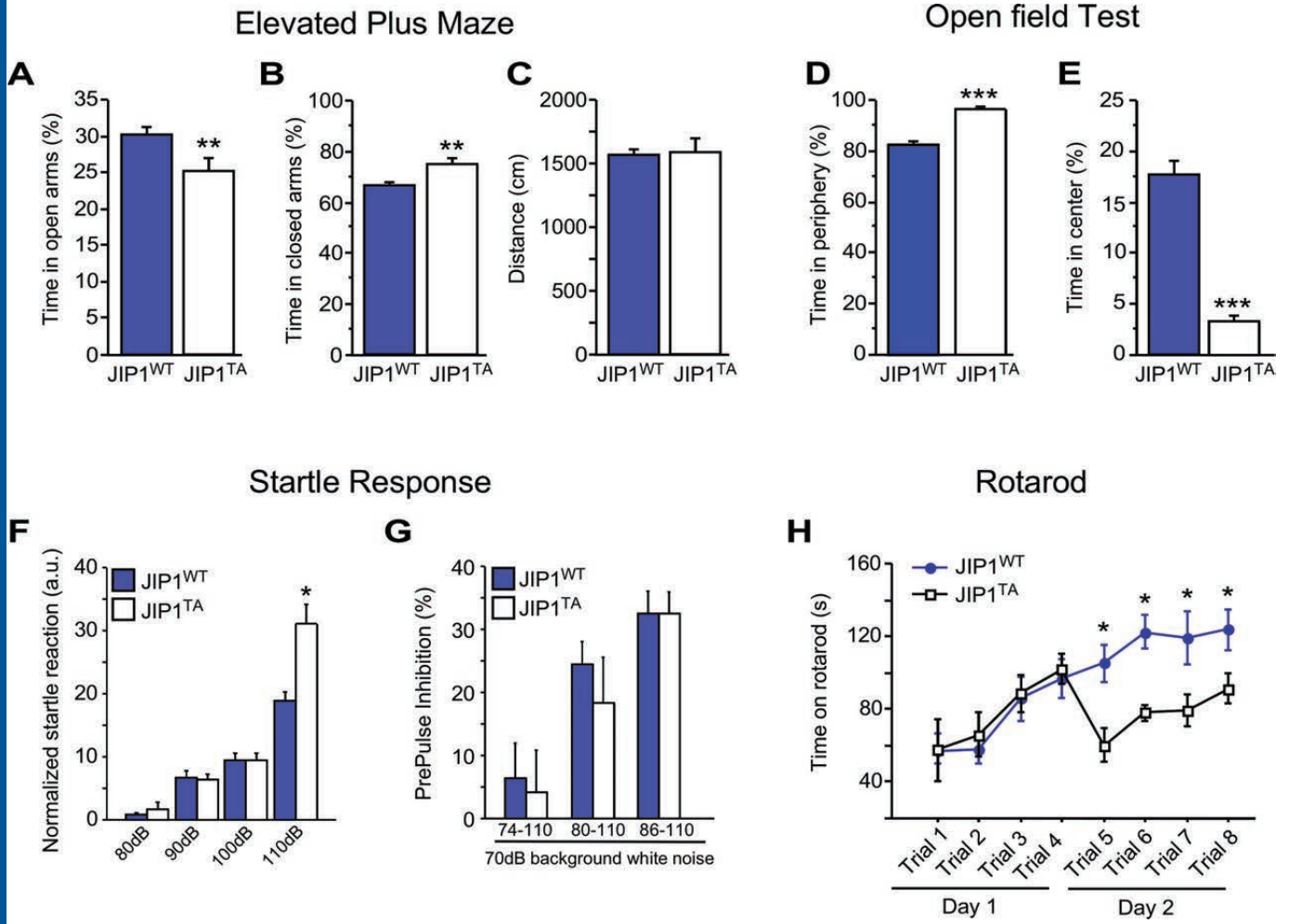


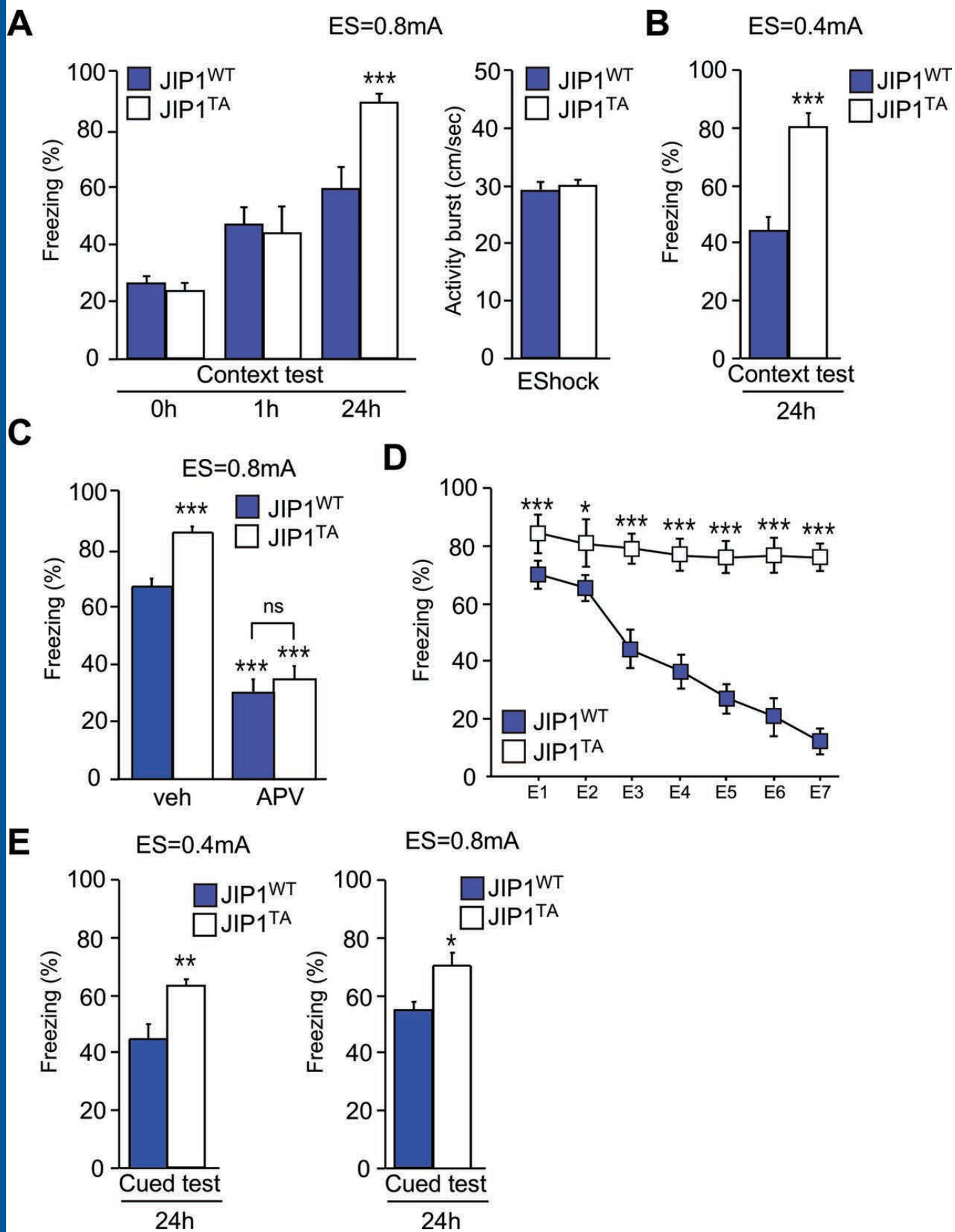


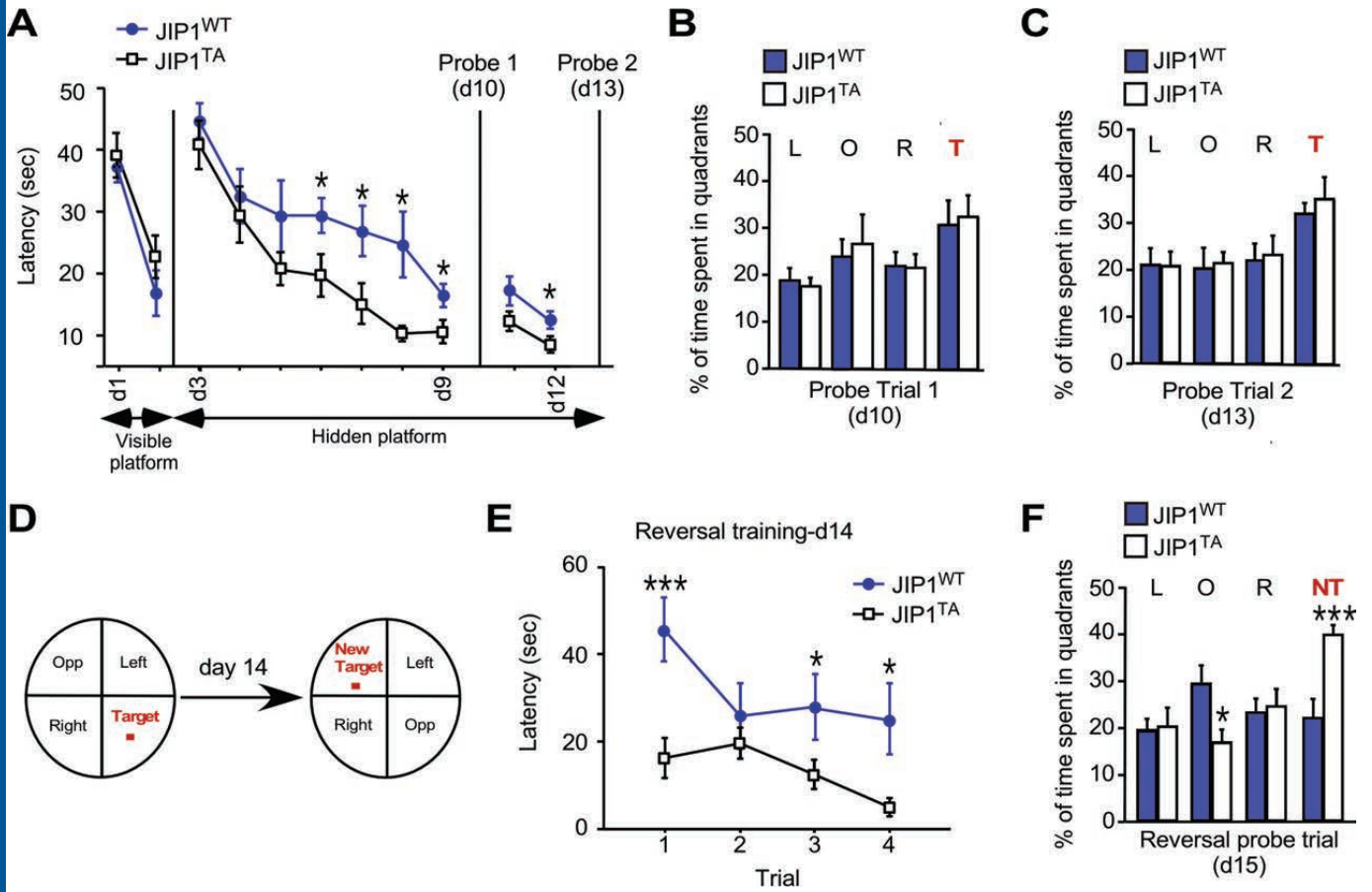


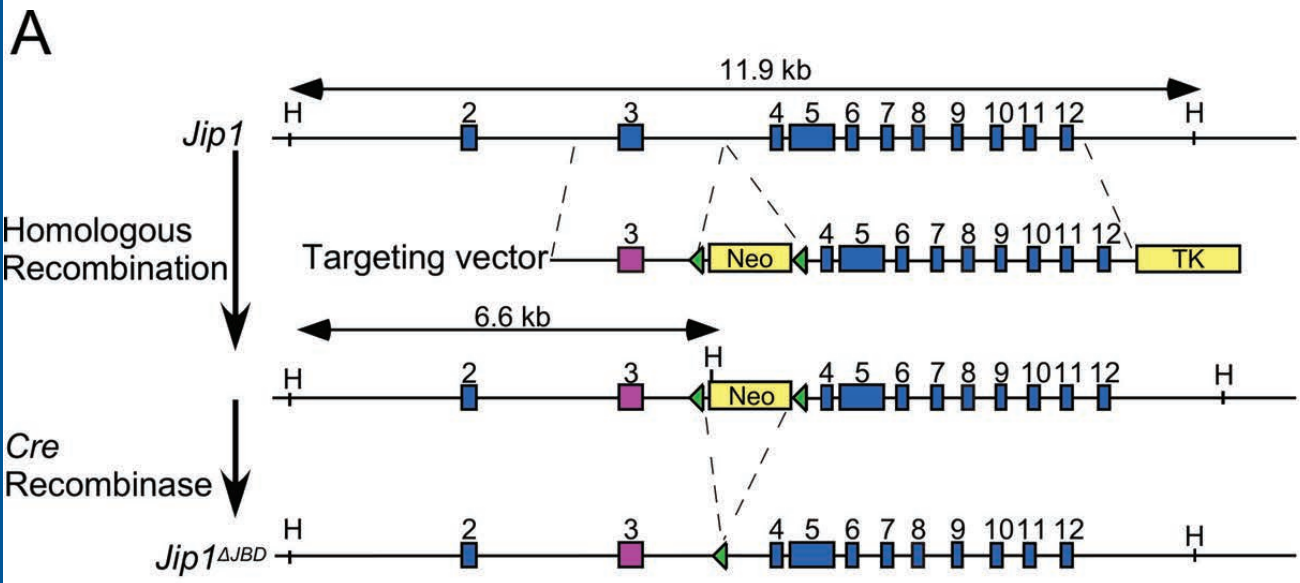












B

Exon III

AGGCCTACCACGCTCAACCTTTTCCCGCAG *Jip1*

R P T T L N L F P Q *Jip1*^{ΔJBD}

--- --- AC**GGCCGCGT**---

G R G

